Future Opportunities in $p+p$ and $p+$A Collisions at RHIC with the Forward sPHENIX Detector

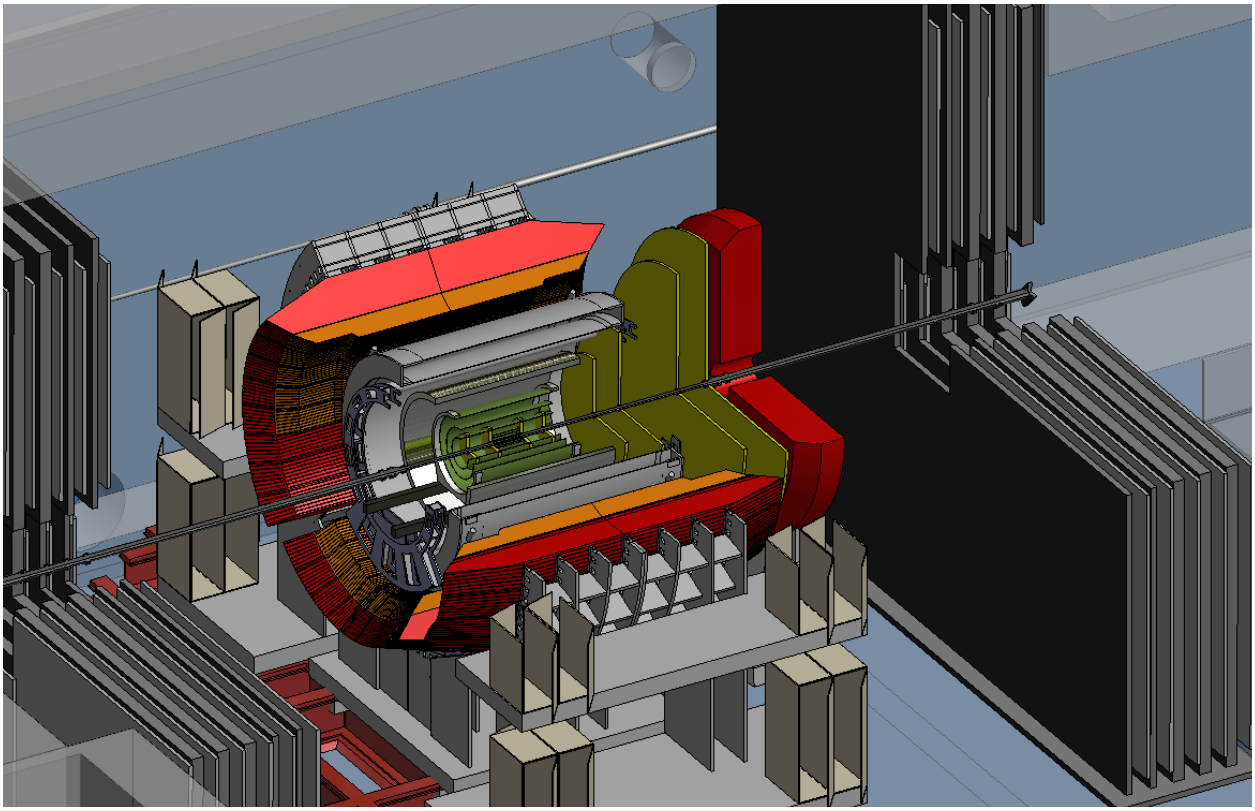

The PHENIX Collaboration

April 29, 2014

Executive Summary

The PHENIX Collaboration presents here its plans for future p+p and p+A running at RHIC in 2021 and beyond, in response to a charge from the BNL Associate Lab Director Berndt Mueller (see Appendix A for the complete charge). The PHENIX collaboration has previously presented plans for the evolution of PHENIX to a next-generation heavy-ion detector (sPHENIX [1]), and ultimately to an EIC detector [2]. The time period covered by the charge is intermediate to these existing proposals and would coincide with scheduled p+p and p+A running at $\sqrt{s_{NN}} = 200$ GeV as part of the proposed sPHENIX run plan.

This proposal focuses on physics observables at forward angles with additional detectors augmenting the sPHENIX upgrade, thus referred to here as "fsPHENIX". With the possibility that in the transition to the EIC the RHIC collider may not maintain the ability to provide hadron collisions, opportunities for significant new discoveries would be lost if the existing investment in RHIC is not fully exploited with measurements in the forward region.

The fsPHENIX physics program centers on a comprehensive set of measurements of jet production in transversely spin-polarized p+p and p+A collisions, exploiting the unique capability of the RHIC collider to provide beams of protons with high polarization in addition to a variety of unpolarized nuclear beams. In p+p collisions we propose a program of intra- and inter-jet measurements designed to separate and elucidate the sources of the large single spin asymmetries measured previously at RHIC for single hadrons. Similar measurements in spin-polarized p+A collisions make use of transverse single-spin asymmetries as a probe of the parton densities in nuclei at small-x. This forward jet physics program can be done with the running already requested for sPHENIX in 2021–2022, and in fact enhances the sPHENIX heavy ion jet program with increased dijet coverage.

In addition, the planned sPHENIX running in p+p and p+A collisions at $\sqrt{s_{NN}}$ =200 GeV will also yield a measurement of the single spin asymmetry for Drell-Yan virtual photons ($2.0 < M < 2.5$ GeV, via the decay to two muons) complementary to the measurement will be made earlier by COMPASS-II. To full realize the physics potential in Drell-Yan, a dedicated running period at 510 GeV will be required in order to yield new, high-statistics Drell-Yan measurements with extended reach into the valence region of the polarized nucleon. By measuring both low-mass and high-mass Drell-Yan muon pairs this dataset will be able to explore and constrain the evolution of Transverse Momentum Dependent

(TMD) functions in the polarized nucleon.

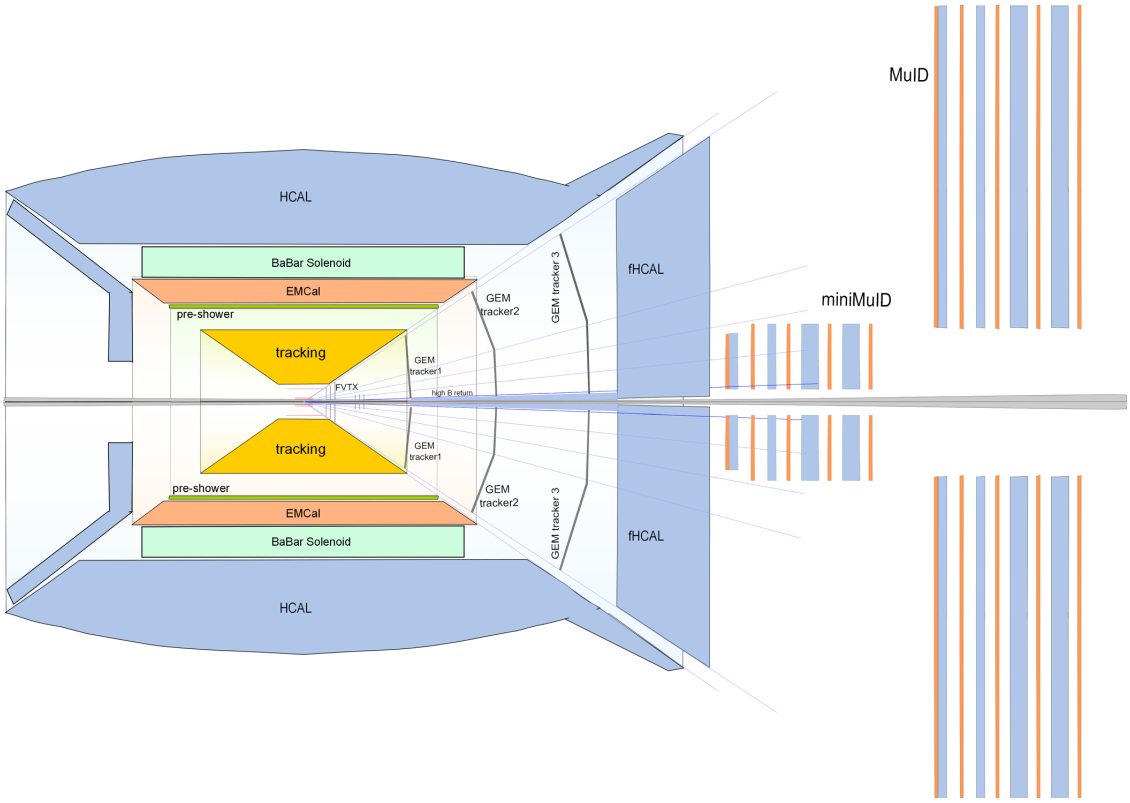

Figure 1: The fsPHENIX detector concept, with the sPHENIX detector as its foundation, takes advantage of the early deployment of technologies and elements of a future EIC detector to enable key p+p and p+A measurements.

In order to optimize the use of available resources, the fsPHENIX detector, as shown in Fig. 1, is developed around the proposed sPHENIX central detector and the re-use of existing PHENIX detector systems (such as the MuID and the FVTX), as well as elements of a future EIC detector forward hadron arm. The majority of the cost of the fsPHENIX detector, estimated to be $12M including overhead and contingency, but not labor, can be viewed as a down payment on an EIC detector that will be needed during the EIC era. About 90% of the cost of the fsPHENIX detector is shared with the EIC detector described in [2]. In addition to providing a important set of new physics measurements that may not be possible in the EIC era, an early investment in fsPHENIX would help provide day-1 readiness of the EIC detector.

In this document we present a set of simulations that outline the capabilities of the proposed fsPHENIX apparatus and the challenges faced by the proposed physics program. The GEANT simulations presented here demonstrated the basic physics measurement capabilities, and need to be followed up with more detailed studies in working towards a full detector design.

This document is organized as follows. Chapter 1 motivates and illustrates the wide spectrum of p+p and p+A physics that can be addressed with the fsPHENIX detector. In Chapter 2 we describe the fsPHENIX detector itself, and in Chapter 3 we show the anticipated performance of the detector for jet and Drell-Yan measurements. Finally, in Chapter 4 we estimate the cost of the fsPHENIX detector systems.

Contents

Chapter 1

Physics Goals

In this section we highlight the key measurements in transverse spin physics and Cold Nuclear Matter that can be pursued with the fsPHENIX detector, with careful attention to what will be known by 2021 and the complementarity of these measurements to those anticipated at the Electron Ion Collider.

A key goal of the study of QCD is to understand the structure of the proton. The observation of large single-spin asymmetries in spin polarized $p+p$ collisions implies a correlation between the spin of the proton and that transverse motion of its constituent partons and offers a window into the structure of a complicated, strongly-interacting many-body state. While spin dependent measurements have been made in Semi-Inclusive Deep Inelastic Scattering (SIDIS) at DESY and CERN, and initial extractions of TMD functions have been made, the connection to spin polarized $p+p$ scattering is difficult theoretically and not fully understood. Because of this, spin-polarized hadron collisions offer key tests of the QCD formalism that has been developed to understand the transverse structure of the proton, and offers the ability to make measurements at higher partonic x where the TMD effects are large. Because RHIC is the world's only polarized proton collider, if these measurements are not made before the transition to the EIC a substantial physics opportunity may be lost.

Another unique capability of RHIC is the ability to provide p+A collisions, both with polarized protons and a wide range of nuclei. Single spin asymmetries measured in the proton direction have been proposed as a tool to access the low-x gluon distribution in nuclei, where saturation effects may play a role. This new opportunity will be partially explored by RHIC in upcoming physics runs in 2015 and 2016, and may warrant a more complete investigation with improved forward instrumentation.

1.1 Jet Production in Polarized Proton-Proton Collisions

Large single transverse spin asymmetries have been observed in hadron-hadron collisions at various energies up to the highest RHIC energies reached so far. Initially these asymmetries were not expected to be large. In perturbative QCD calculations such asymmetries would require a helicity flip and a phase and are thus suppressed by the small mass of a parton with respect to the scale and the strong coupling α_S [3]. Since then it has be found that higher twist contributions, while initially suppressed by the hard scale, can create sizable effects capable of describing these large asymmetries [4, 5, 6, 7, 8, 9, 10]. The single spin asymmetries are defined as azimuthal asymmetries in the yield of particles:

$$A_N = \frac{N^{\uparrow}(\phi) - N^{\downarrow}(\phi)}{N^{\uparrow}(\phi) + N^{\downarrow}(\phi)} \quad , \tag{1.1}$$

where generally the cosine modulation is studied. The azimuthal angle ϕ is defined from the direction perpendicular to the transverse spin direction of the polarized beam with respect to the polarized beam's direction.

Various higher twist contributions to these single spin asymmetries exist which can be generally classified into initial state and final state effects. In both, correlation functions exist between gluonic and fermionic contributions which, unlike distribution functions, contain combinations of three fields instead of two, such as $< PS|\overline{\psi}F\psi|PS >$. The corresponding contributions for pion single spin asymmetries can be classified as:

$$\begin{aligned}
\frac{d^2\sigma}{d^2P_T} &\propto h_1^a(x_1) \otimes f_1^b(x') \otimes \sigma(ab \to c) \otimes \hat{E}_F^{c,h}(z_1, z_2) && (1.2)\\
&+ G_F^{qg}(x_1, x_2) \otimes f_1^b(x') \otimes \sigma'(ab \to c) \otimes D_{1,c}^h(z) && (1.3)\\
&+ G_F^{ggg}(x_1, x_2) \otimes f_1^b(x') \otimes \sigma''(ab \to c) \otimes D_{1,c}^h(z) \quad , && (1.4)
\end{aligned}$$

where $f_1(x)$, $h_1(x)$ and $D_1(x)$ are the (leading) Twist-2 unpolarized and transversity distributions and the unpolarized fragmentation function respectively. The terms $\hat{E}_F^{c,h}(z_1, z_2)$ corresponds to the higher twist final state contribution and the terms $G_F^{qg}(x_1, x_2)$ and $G_F^{ggg}(x_1, x_2)$ correspond to the higher twist quark-gluon and three gluon correlation functions. Schematically these contributions are depicted Figs. 1.1.

Some of the higher twist pieces can be related to transverse momentum moments of the transverse momentum dependent distribution and fragmentation functions (TMDs)[11], most importantly the Sivers and Collins [10] functions. For this reason the initial and final state parts of the asymmetries are often referred to as Sivers-like and Collins-like although the higher twist picture is clearly the appropriate one in this single-scale problem. The main question is how much each effect is actually contributing to these large pion asymmetries.

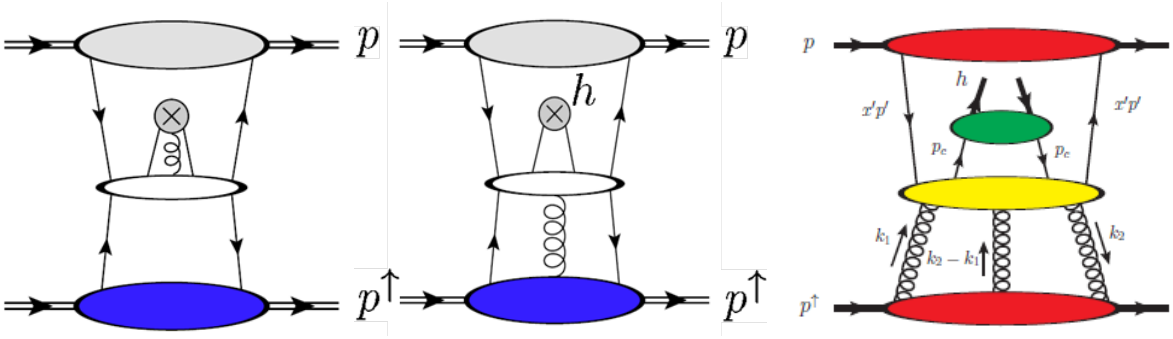

Figure 1.1: Higher twist diagrams contributing to the large single spin asymmetries from hadrons in transversely polarized p+p collisions. Left figure: Higher twist fragmentation contribution; middle figure: quark-gluon correlator; right figure: tri-gluon correlator.

1.1.1 The sign mismatch *problem*

Based on the connection to the TMDs, which are reasonably well measured in semi-inclusive DIS but at generally smaller partonic x, some extrapolations can be made. A large sign mismatch is found when only taking into account the higher twist contribution related to the Sivers function [12]. This can have various reasons:

- The most obvious option is that all the other possible contributions to these asymmetries do actually contribute substantially and there is no sign-mismatch problem at all.
- The Sivers function could contain a node in transverse momentum which was not accessible in the SIDIS measurements so far. This option is ruled out as both HERMES and COMPASS measure to transverse hadron momenta of more than 1 GeV at which point a TMD description would anyway become less applicable.
- The Sivers function could have a node in x between the covered regions in SIDIS ($\sim$0.01-$\sim$0.3) and p+p ($\sim$0.4-$\sim$0.6).
- Some completely different process such as diffraction is responsible for the majority of the large transverse single spin asymmetries.
- TMD factorization breaking itself may lead to new spin asymmetries [13, 14].

In order to address this, several measurements have been proposed.

1.1.2 Initial state related measurements

The main measurements predominantly sensitive to the initial state effects are jet and direct photon final states as both of those are insensitive to the asymmetries which are

created in the fragmentation. Direct photon measurements are expected to be made with the MPC-EX. For jet measurements initial indications show [15] that the asymmetries are small, which might be an indication that the initial state contribution to the large pion single spin asymmetries is small. However, a somewhat skewed selection of Sivers function parameterizations from the SIDIS data [16] claims to be able to describe both the large pion single spin asymmetries and the relatively small jet asymmetries [17], see Figs. 1.2.

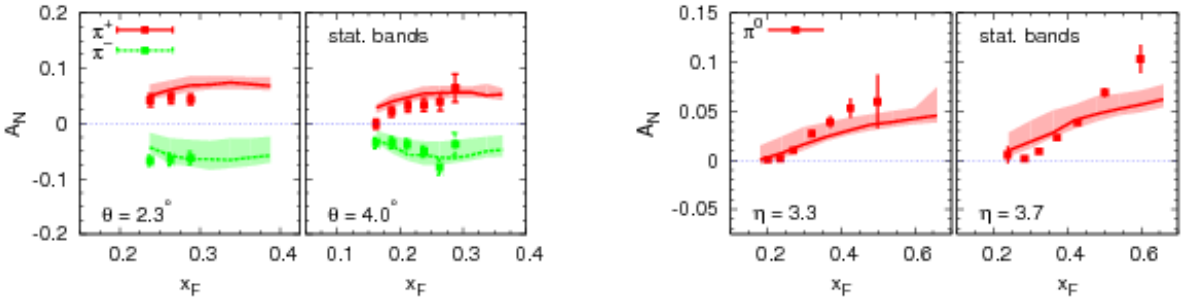

Figure 1.2: Left: Single spin asymmetries A_N for charged pions from Brahms. Right: neutral pions from STAR together with the best parameterization based on the Sivers function from SIDIS.

The argument is that a partial cancellation of the u and d quark Sivers functions can make this possible as shown in Fig. 1.3. In particular they suggest that enhancing the jet measurements towards u or d quark initiated jets via requiring a high-z charged pion in that jet could then show sizable asymmetries. The fsPHENIX upgrade will attempt to address these predictions and determine if the individual quark contributions are indeed as large as suggested. A different prediction, still based on the SIDIS Sivers fits but using the actual relation to twist-3 distribution functions, finds similar sizes but opposite signs [18].

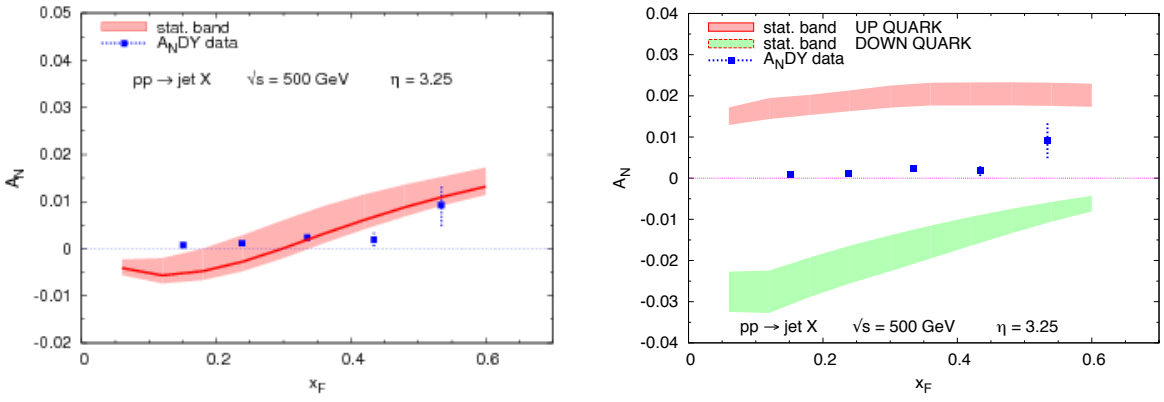

Figure 1.3: AnDY single spin asymmetries together with the best parameterization based on the Sivers function from SIDIS displayed separately for jets originating from u and d quarks (right) and combined (left).

1.1.3 Final state related measurements

While only higher twist fragmentation effects enter in the measured large pion single spin asymmetries, those can be partially related to the transversity distribution and the transverse momentum moment of the Collins fragmentation functions. The Belle, HERMES and COMPASS measurements have clearly established [19, 20, 21, 22, 23, 24], that both Collins fragmentation functions and up and down quark transversity distribution functions exist. The most recent extraction can for example be seen in Fig. 1.4 as obtained in [25]. However,

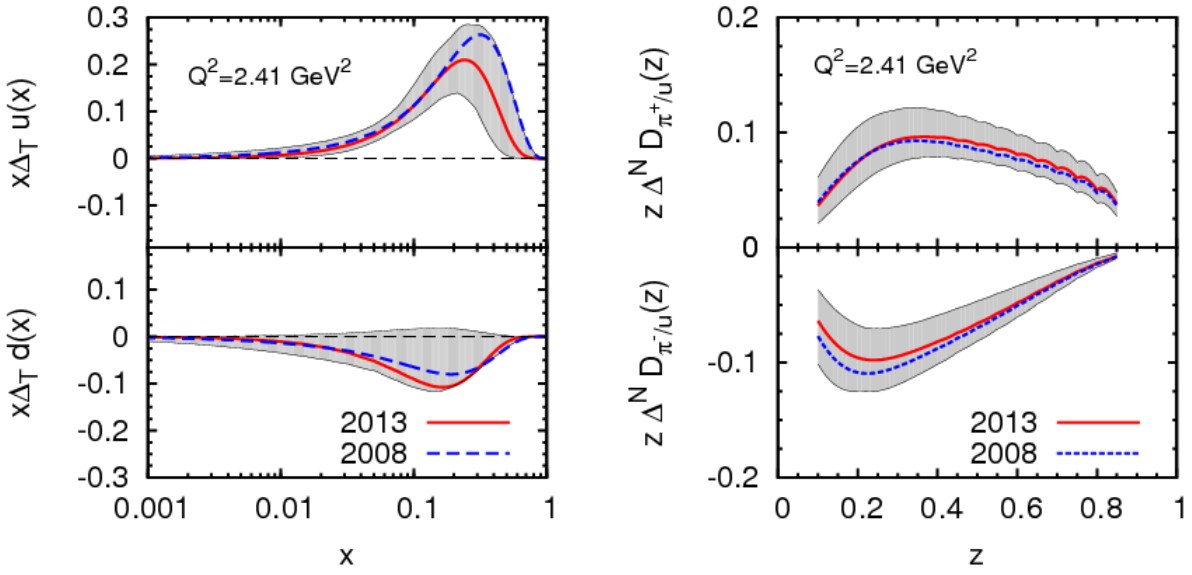

Figure 1.4: Left: Up and down quark transversity distributions as a function of x as obtained from the latest global transversity analysis. Right: Favored and disfavored Collins fragmentation functions from the same global analysis.

the x range probed in the large p+p single spin asymmetries (0.3-0.6) has not been accessed and is only roughly constrained by the functional form of the global transversity and Collins fits as well as positivity bounds[26]. The actual Collins effect, i.e. the TMD and not the corresponding higher twist counterpart, can actually be accessed in transversely polarized proton-proton collisions when measuring transverse spin asymmetries in the azimuthal modulation of pions around the jet axis it belongs to.

Measuring these asymmetries at forward rapidities together with the known Collins fragmentation functions allow to access the transversity distributions in an x range not probed so far and in exact overlap to the range probed in the proton-proton A_N's. This will allow the extraction of the tensor charge for up and down quarks without the need of extrapolation to x above 0.3. Furthermore the direct impact of these final state induced

asymmetries on the simple pion A_N's can be tested at the same time by requiring the same selection for both Collins and simple asymmetries. The addition of kaon identification would allow a more detailed flavor decomposition of the transversity distribution including sea components and shed light on the surprising kaon asymmetries observed by Brahms [27] with similar asymmetries for both charges. Naturally, the related interference fragmentation function measurements could be carried out as well.

1.1.4 Diffractive measurements

Some recent school of thought connects the transverse single spin asymmetries not to hard initial state or final state effects but potentially through a diffractive contribution. Some preliminary data from STAR where the size of the asymmetries for π^0 in conjunction with electromagnetic clusters indicate larger asymmetries in the absence of additional activity. Also the large very forward neutron asymmetries could be explained by diffractive causes. Typically diffractive events manifest themselves by hadronic activity with a large rapidity gap to any other detector activity. Consequently isolated pions in the absence of higher multiplicity jets would enhance such diffractive events and with otherwise good jet detection capabilities one could study the size of charged pion asymmetries in such special event topologies. If a large contribution to the single spin asymmetries is coming from diffractive processes, the asymmetries would need to be large for those diffractive enhanced events while smaller for regular jet related events.

1.1.5 Expected knowledge by 2021

The π and jet asymmetry measurements have been performed already in STAR, Brahms and PHENIX for the pions and AnDY for the jets. However, so far no experiment has the capabilities to reconstruct jets in the forward direction and also detect charged hadrons in the same region and correlate with these jets. STAR has currently only neutral meson capabilities in the forward regions and therefore their jet related studies are based on "neutral" jets in an electromagnetic calorimeter.

The PHENIX MPC-EX upgrade will give prompt photon capabilities to PHENIX in 2015-2016, which are another important venue in understanding the origin of the large pion single spin asymmetries (see Figure 1.5). Prompt photon measurements with the MPC-EX may point the way for further investigations with fsPHENIX, but will not provide a definitive measure of the fragmentation contributions to the single particle A_N's. The MPC-EX may also have π^0 Collins measurements based on mostly neutral jets as well.

The capabilities of fsPHENIX will be unique in reconstructing real jets with a hadronic calorimeter and the ability to detect charge separated hadrons within it.

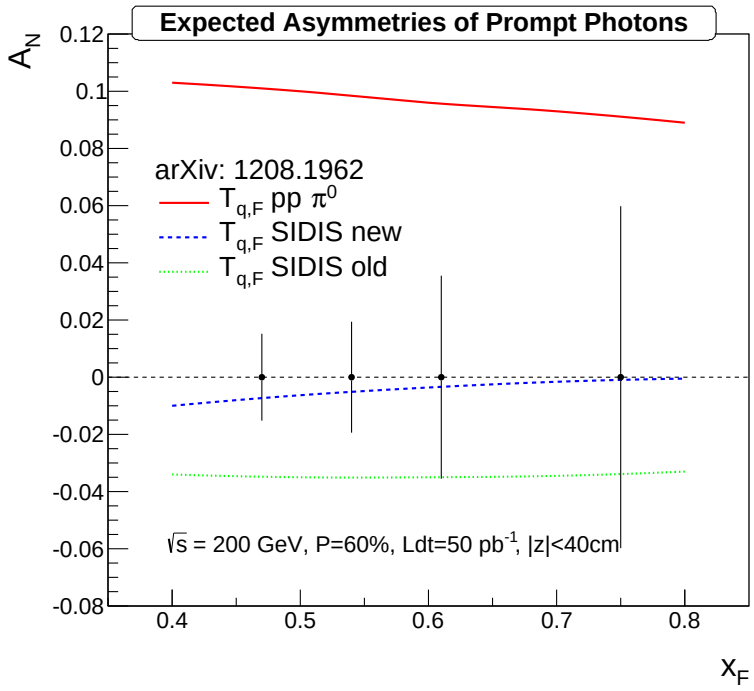

Figure 1.5: Projected prompt photon single-spin asymmetries from the PHENIX MPC-EX detector.

1.2 p↑+A Collisions

1.2.1 Investigating the Properties of Cold Nuclear Matter

Measurements of particle and jet production in proton-nucleus collisions at forward angles with fsPHENIX at $\sqrt{s_{NN}} = 200$ GeV allow the study of fundamental properties of Quantum Chromodynamics (QCD) at an intermediate parton fractional momentum x (x_1 in the proton) and at a high gluon densities at low-x (x_2 in the nucleus).

In high energy heavy-ion collisions a state of hot, dense medium of strongly interacting quarks and gluons, i. e. the Quark Gluon Plasma (QGP), is formed. In order to interpret the measurement of the hot nuclear medium and to understand the detailed properties of the QGP, the initial state properties of the Cold Nuclear Matter (CNM) need to be well-understood first. One of the main goals of fsPHENIX's p+A measurements is to use spin-independent, as well as spin-dependent observables, to address issues such as gluon saturation effects such as the Color Glass Condensate (CGC) [28], parton (quark and gluon) densities modifications in CNM [29], parton propagation through CNM including parton splitting, radiative energy loss and coherent multiple scattering, and modification of parton fragmentation process in CNM.

In addition to measuring charged hadron production, the fsPHENIX detector will allow us to directly measure jets in the forward direction and compare the fragmentation functions

in different hard-collision systems of p+p and p+A. This provides us with a powerful tool to clearly separate the non-perturbative fragmentation effects from that of QCD-dynamic effects, such as gluon saturation, shadowing, Cronin effect, parton energy loss and coherent multiple scattering. This unique (at RHIC) forward jet detection capability will allow us to better identify effects such as suppression of the away-side jet in jet-jet, jet-hadron and hadron-hadron correlations. When combined with the RHIC collider's flexibility of colliding different species of nuclei in from p+C, p+Si to p+Au, effects the nuclear density can be clearly isolated.

While the recent p+Pb collision data at $\sqrt{s_{NN}} = 5.02$ TeV from CMS, ALICE [30] and LHCb Collaborations at LHC have generated significant excitement, RHIC is planning to conduct its first p+Au collisions at $\sqrt{s_{NN}} = 200$ GeV in FY2015. Due to the center of mass energy differences, RHIC at $\sqrt{s_{NN}} = 200$ GeV while LHC at $\sqrt{s_{NN}} \geq 5$ TeV, fsPHENIX will cover a very different kinematic regime when compared to the LHC. Specifically, fsPHENIX accesses a transition regime with gluon momentum fraction x_g=$10^{-3} \sim 10^{-2}$, the expected region for the onset of gluon saturation, while LHC experiment accesses x_g=$10^{-5} \sim 10^{-4}$, at this x the relevant Q^2 will be much larger than the saturation scale [31]. Furthermore, while forward jets in fsPHENIX at RHIC will be dominated by quark-gluon hard scattering between a valence quark from proton (x_1=0.1$\sim$ 0.6) and a gluon from the nuclei (x_2=$10^{-3} \sim 10^{-2}$), jet production at LHC are dominated by gluon-gluon hard scattering. Therefore, due to this kinematic differences, the underlying hard scattering as well as the subsequence QCD processes in p+A collisions are quite different between fsPHENIX at RHIC and current experiments at the LHC.

At RHIC, the success of stochastic cooling in the storage ring makes small emittance ion beam possible and a new ion source (EBIS) provides an unprecedented flexibility of colliding a beam of nuclei (^{12}C, ^{28}Si, ^{64}Cu, ^{197}Au and ^{208}Pb etc.) with a beam of protons. In early 2013, the RHIC community realized that the new machine capability offers an unique probe to study properties of cold nuclear matter and high density gluon phenomena in nuclei, and to access a transition regime to observe the onset of gluon saturation. Most importantly, unique only to the RHIC machine, the proton beam at RHIC is routinely polarized with an average polarization of 60%. Therefore, In addition to R_{pA} type observables in single-hadron, inclusive jet, di-jets and Drell-Yan production channels, fsPHENIX will provide the first detailed transverse Single-Spin Asymmetry (A_N) measurements in p$^{\uparrow}$+A collisions.

The combined sPHENIX/fsPHENIX detector, with jet reconstruction over a wide range of central and forward rapidities, will be capable of a wide array of physics measurements in p+A collisions:

- $A_N^{h^{\pm}}$ in p$^{\uparrow}$+A
- A_N^{jet} in p$^{\uparrow}$+A
- A_N^{jet} in "high-z tagged jet" events in p$^{\uparrow}$+A

- R_{pA}^{h}
- R_{pA}^{jet}
- jet p_t broadening in $p + A$
- di-jets and hadron-jet correlations (CGC inspired disappearance of away-side jet)
- gamma-jet correlations
- Drell-Yan R_{pA}

1.2.2 Transverse Single-Spin Asymmetries in p$^{\uparrow}$+A Collisions

Recently, there have been exciting theoretical and experimental advances in understanding how to exploit spin observables to study gluon saturation at RHIC, by colliding a transversely polarized proton beam on an unpolarized heavy ion beam. Both PHENIX and STAR experiments are already in preparation for p$^{\uparrow}$+A collisions starting in Run-2015, to carry out such a new physics program using current detectors and near-term upgrades.

Large transverse single spin asymmetries (TSSAs), $A_N \sim 10\%$, defined as the difference of yields with the proton's spin flipped divided by the sum, have been observed in the production of various high energy hadron production (such as pions, kaons, etc.) in polarized proton-proton collisions at RHIC. The observed asymmetries are most pronounced in the forward region along the polarized proton beam, corresponding to collisions between a large momentum quark from the polarized proton and a soft gluon from the opposite, unpolarized, proton. In a collision of a polarized proton with an unpolarized nuclei, this soft gluon would come from the nuclei. In a recent study, Kang and Yuan predict [32] that the ratio of the spin asymmetry TSSAs of an ion beam over a proton beam will have the following asymptotic behavior:

$$\left.\frac{A_N^{pA\to h}}{A_N^{pp\to h}}\right|_{P_{h\perp}^2 \ll Q_s^2} \approx \frac{Q_{sp}^2}{Q_{sA}^2} e^{\frac{P_{h\perp}^2 \delta^2}{Q_{sp}^4}} , \quad \left.\frac{A_N^{pA\to h}}{A_N^{pp\to h}}\right|_{P_{h\perp}^2 \gg Q_s^2} \approx 1 . \tag{1.5}$$

That is, the ratio of nuclear and nucleon TSSAs for inclusive production of single hadrons of momentum $P_{h\perp}$ at forward rapidity directly probes soft gluons in the colliding heavy ion, and is immediately sensitive to the saturation scale of both the proton and the nucleus. It is expected that the larger the nucleus A, the larger the saturation scale. Thus a set of measurements with various nuclear species will shed new light on our understanding of the gluon evolution inside the nucleus at saturation. RHIC is the only collider in the world with high-energy polarized proton beams, and with the flexibility of colliding almost any desired ion beam (C, Si, Cu, Au, Pb etc.) enabled by the Electron Beam Ion Source (EBIS).

RHIC is in a unique position to use spin observables to explore this novel uncharted regime of condensed and saturated gluons.

1.2.3 Expected knowledge by 2021

The PHENIX collaboration, with its forward calorimeter upgrade project underway (MPC-EX), is focusing on measurements of the forward prompt photon production through the quark-gluon Compton process in order to extract gluon densities in nuclei (see Figure 1.6). A great deal of what will be interesting to be pursued in 2021-22 will determined by the measurements made by PHENIX and STAR in 2015-16. However, neither STAR nor PHENIX have the capability to measure forward charged hadron (or jet) production at $\eta > 2.2$. In contrast, the fsPHENIX upgrade will cover a forward rapidity for jet at $1.7 < \eta_{jet} < 3.3$ and for charged hadrons at $1.2 < \eta < 4.0$.

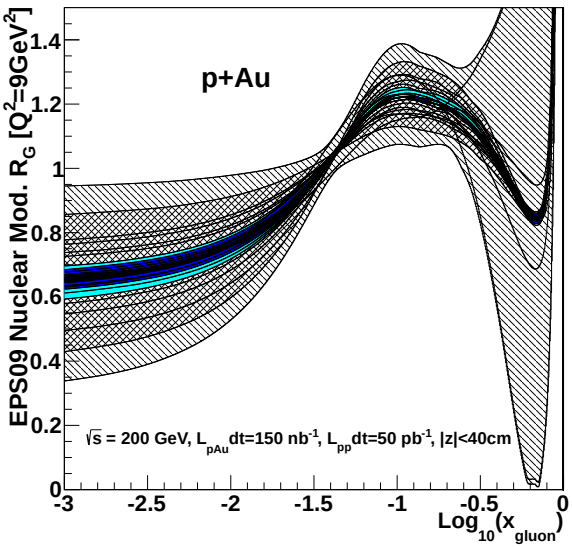

Figure 1.6: Projected improvements on the EPS09 [29] model of gluon shadowing in nuclei. The interior blue band represents the constraints with the MPC-EX anticipated dataset at the one-sigma level, while the outer blue band represents the 90% confidence level.

The PHENIX MPC-EX will make initial measurements of the suppression of single hadron spin asymmetries for π^0 mesons in 2015-6 (see Figure 1.7). These measurements will be a first, initial examination of the physics potential of the use of single spin asymmetries to probe the nuclear gluon density, and will determine if the physics warrants further investigation with a wider array of observables.

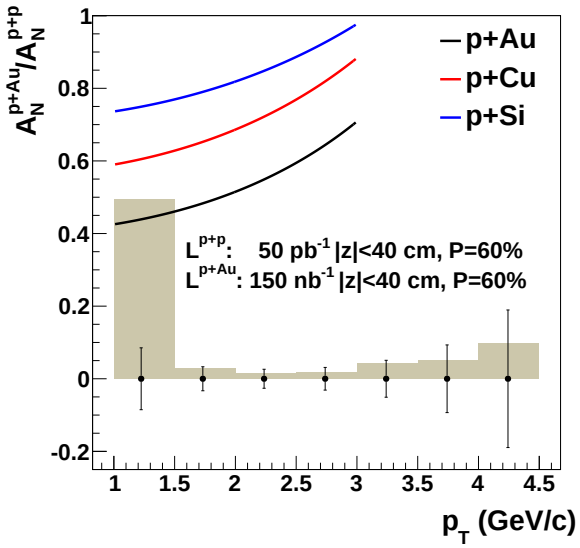

Figure 1.7: Projected error bars on the ratio of π^0 single-spin asymmetries in p+p and p+A collisions from the PHENIX MPC-EX detector, assuming 50pb^{-1} integrated luminosity for p+p, 150nb^{-1} for p+A, and 60% polarization. The lines are schematic and indicate the potential pattern of suppression for a variety of p+A species, following [32].

1.3 Drell Yan

1.3.1 Modified Universality of the Sivers Function

The Sivers function $f_{1T}^{\perp}(x, kt)$ [33] was initially suggested as a possible mechanism to explain the large transverse single spin asymmetries observed in hadron-hadron collisions. Initially it was claimed to be a time reversal-odd function and thus zero by Collins [34]. However, after an explicit model example was found to create such a function [35] it was realized [36], that the gauge invariance of the bi-local operator requires gauge links which cannot be ignored in the same way as for collinear distribution functions. These gauge links introduce a simple non-universality in the form of a sign change depending whether these gauge links need to be connected at positive or negative light-cone infinity. Consequently the Sivers function extracted from semi-inclusive DIS and the Sivers function in the Drell-Yan process are supposed to be of opposite sign [37].

$$f_{1T}^{\perp}(x, kt, Q^2)|_{\mathrm{DY}} = -f_{1T}^{\perp}(x, kt, Q^2)|_{SIDIS} \quad . \tag{1.6}$$

Naively one can interpret the role of the gauge links as some form of re-scattering of the participating partons on either the same or opposite proton remnants. Consequently in the SIDIS case the same remnant is of opposite color-charge than the struck quark and this re-scattering would be attractive while in the DY case the opposite remnant is of same color-charge and the re-scattering would be repulsive, and hence the Sivers function

changes sign between the two processes, in contrast the usual 'universal' behavior of distribution functions.

The test of this prediction is of great importance to confirming the existing theoretical picture of how these so-called naive time-reversal odd distribution functions are created and the role of gauge invariance in parton distribution functions. If this prediction is not borne out by experimental data it will require the development of a completely new way of thinking about such distribution functions.

Since the existence of the Sivers function has been well established in SIDIS [21, 22] it is important to confirm the sign change by making the corresponding Drell-Yan measurement of the single spin asymmetries:

$$A_{DY}^{\phi_S} \propto \frac{\sum_q e_q^2 f_{1T,q}^{\perp}(x_1, kt_1) f_{1,\bar{q}}(s_2, kt_2)}{\sum_q e_q^2 f_{1,q}(x_1, kt_1) f_{1,\bar{q}}(x_2, kt_2)} \quad , \tag{1.7}$$

where f_1 are the unpolarized parton distribution functions and proton 1 is polarized. This requires the Sivers asymmetry be measured in the x region in the polarized proton ($x > 0.1$) where the Sivers function is large and a transverse virtual photon momenta low enough that the TMD formalism (two scales: $Q \gg Q_T \approx O(\Lambda_{QCD})$ is applicable, in contrast to the higher twist formalism (which has a single, hard scale). The expected size of the Drell-Yan single spin Sivers asymmetry before evolution, based on the global analysis of the SIDIS data is shown in Fig. 1.8 for $\sqrt{s}$ =200 GeV polarized proton-proton collisions as calculated by Anselmino [38].

1.3.2 QCD evolution of TMDs

In Drell-Yan the hard scale of the process is given by the invariant mass of the lepton pair and traditionally selected between the J/ψ and Y resonances. This is generally higher than the average scales of the SIDIS measurements of $Q^2 = 2.4$ GeV and $Q^2 = 3.1$ GeV in HERMES and COMPASS respectively, although COMPASS' highest x_{Bj} points are comparable. As a consequence one has to take into account the QCD evolution of the Sivers function and one cannot in general expect to measure the same magnitude but only a relative sign of the Sivers functions from SIDIS and DY. Recently theorists have also started to calculate the scale dependence of transverse momentum dependent distribution functions [39]. While the theoretical approach is similar between theorists, the choice and method of extracting non-perturbative factors from other unpolarized measurements result in differing predictions. In the worst case a maximally 8% asymmetry without TMD evolution would become 1% [40, 41, 42, 43]. Given the generally limited statistics for the Drell Yan process this will make the sign change test substantially more challenging. Partially motivated by the potentially low asymmetries and the lower statistics a low mass DY measurement below the J/ψ mass at around 1.5–2.5 GeV is considered for fsPHENIX, in addition to the more traditional high mass (4.0-9.0 GeV) measurement.

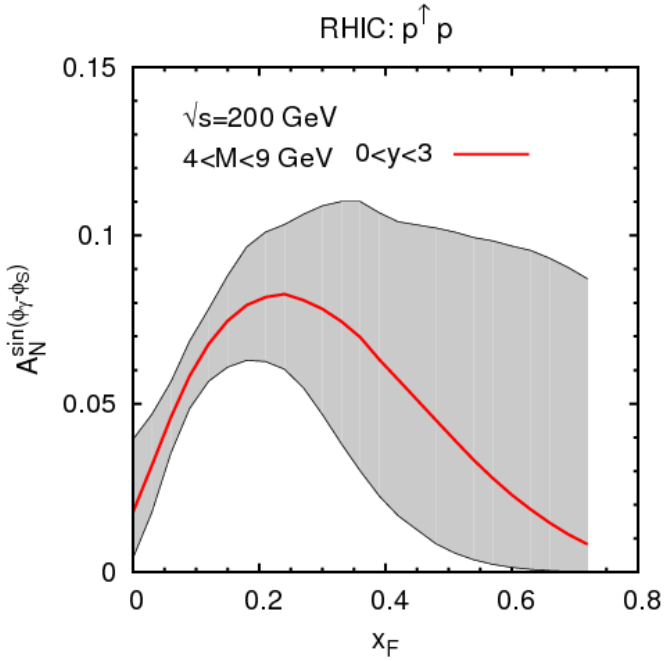

Figure 1.8: Drell-Yan Sivers asymmetries for $\sqrt{s}$ =200 GeV polarized p+p collisions as a function of the virtual photon's x_f. The effects of evolution on the magnitude of the asymmetry have not been accounted for in this prediction.

1.3.3 Expected knowledge by 2021

The COMPASS experiment is in the process of preparing an upgrade (COMPASS-II) which utilizes a 190 GeV π^- beam and a transversely polarized proton NH_3 target. In this experiments, Drell-Yan lepton pairs will be produced predominantly from valence partons in the pion and proton, which makes it possible to access the Sivers function in the x region of interest.

The anticipated COMPASS-II running schedule foresees about one year of data-taking which could provide a definitive measurement of the sign change, assuming TMD evolution effects are small. However, the smaller the asymmetries become through evolution, the less definitive such a measurement would be. In any case RHIC will be the only other place where the sign change of the Sivers function can be studied in the foreseeable future and even a non-definitive COMPASS measurement would go unconfirmed without RHIC. In addition, the fsPHENIX spectrometer will allow access to significantly higher partonic x in the polarized nucleon. A detailed comparison of the COMPASS-II and fsPHENIX measurements can be found in Section 3.3.

Chapter 2

Detector Concept

The fsPHENIX detector is built upon two key foundations - the sPHENIX central detector, which is optimized for the detection and measurement of jets at central rapidity, and the EIC detector forward hadron arm. While sPHENIX is anticipated to be commissioned and ready for physics data taking in 2021, we anticipate some EIC detector elements as being moved earlier in time for fsPHENIX. In this way we take advantage of significant integration of the sPHENIX/fsPHENIX/EIC detectors in a cost-effective manner. Additional instrumentation (such as the FVTX and the MuID) are carried over from the original PHENIX detector, making efficient use of existing resources.

In this section we describe the various detector subsystems in the fsPHENIX detector and their performance requirements.

2.1 fsPHENIX Detector Overview

The proposed fsPHENIX detector builds on the solid foundation of the sPHENIX detector [1] and is integrated with the flux return from the sPHENIX detector in a combined design. The combination of sPHENIX and fsPHENIX provide an experimental platform that is greater that the sum of its parts, with wide kinematic coverage for jets. In addition, many of the forward detector elements in fsPHENIX are common with the proposed EIC detector [2], providing an efficient upgrade path from RHIC to the Electron Ion Collider.

The conceptual design for the combined sPHENIX/fsPHENIX detector is shown in Figure 2.1. A magnetic field for particle tracking and charge identification is provided by shaping the sPHENIX superconducting solenoid field with a steel piston located around the beam line and an iron return yoke designed as part of the hadronic calorimeter. High resolution tracking near the interaction point is obtained from a reconfigured version of the existing FVTX detector. Three new GEM stations provide intermediate tracking and excellent momentum determination for charged particles. A hadronic calorimeter

measures total jet energy, position and size. The GEM tracker and hadronic calorimeter are identical in design to those proposed for the EIC detector forward hadron arm.

The existing PHENIX North Muon Identifier (MuID) system, covering $1.2 < \eta < 2.4$, is used for muon identification. We propose to extend the pseudo-rapidity region for muon identification from $\eta = 2.4$ to $\eta = 4$, by building a "miniMuID" with a design similar to the existing PHENIX MuID.

To summarize, the subsystems which are reused in this proposal from existing PHENIX and the proposed sPHENIX:

- The sPHENIX superconducting solenoid
- The PHENIX Forward Vertex Tracker (FVTX), in a new configuration
- The PHENIX North Muon Identifier (MuID)

The new detector subsystems to be built as part of fsPHENIX and a future EIC detector include:

- A forward hadronic calorimeter
- Three stations of GEM trackers
- The "miniMuID", for muon identification at high pseudorapidity
- A magnetic field shaper for the forward region

The baseline fsPHENIX design could be upgraded with a RICH detector (the one designed for the EIC detector built around sPHENIX [2] perfectly fits the outlined physics goals) to provide charged kaon and pion identification. Such and addition would allow exciting new physics measurements, such as the Collins asymmetry for identified particles in jets. However, we do not consider this option in detail in this paper.

2.2 Magnet System

As with sPHENIX, the magnetic field for charged particle tracking is provided by the BaBar superconducting solenoid with a 1.5 tesla longitudinal magnetic field. The BaBar magnet is designed to have higher current density at both ends to maintain high field uniformity along the magnet axis. This design also enhances the momentum analyzing power in the forward region. However, the transverse component of the field B_T drops rapidly at pseudorapidities $\eta > 3$. To further enhance the momentum measurements in the very forward acceptance, we propose a passive magnetic material piston surrounding the beam

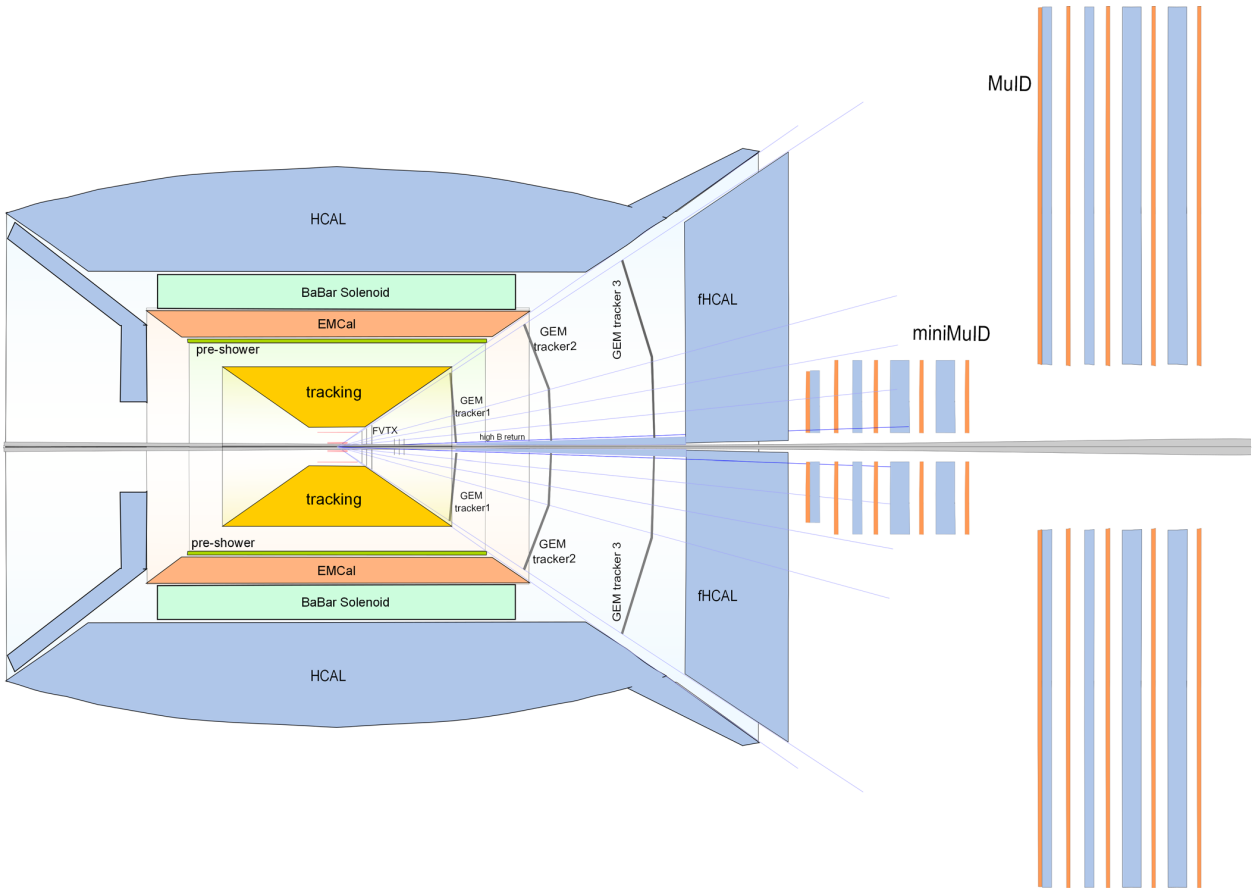

Figure 2.1: A schematic view of combined sPHENIX/fsPHENIX detector systems, showing the location of vertex tracker (a reconfigured FVTX), intermediate tracker (GEM), HCal, MuID, and piston field shaper in the forward region.

pipe to shape the magnetic field near the beam axis, see Figure 2.2. One possible choice for a large saturation point material for such a field shaper could be an alloy with a large concentration of cobalt. For example, the material HIPERCO-50 with a 49%Co+49%Fe composition saturates at 2.25 Tesla.

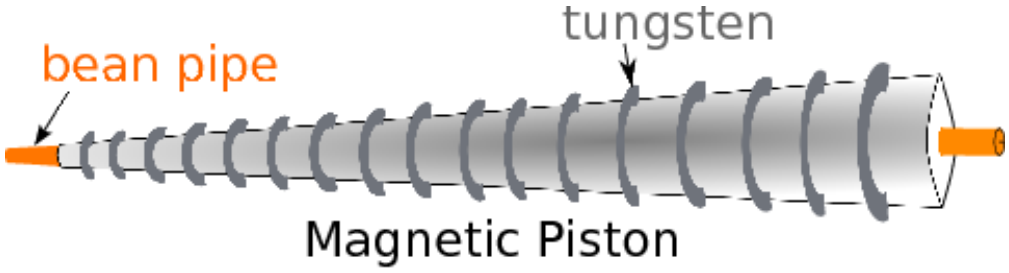

Figure 2.2: The magnetic piston field shaper surrounding the beam pipe. The tungsten saw-tooth ring structure is also shown, as a possible upgrade to the baseline design to absorb the background from the particles shower within the piston material.

Figure 2.3 shows the magnetic field configuration and demonstrates how the field is distorted by the piston field shaper, improving the analyzing power for charged track measurements at high rapidity. Figure 2.4 presents the calculated momentum resolution under different assumptions, demonstrating resolution improvement by more than a factor of two at $\eta > 3.5$.

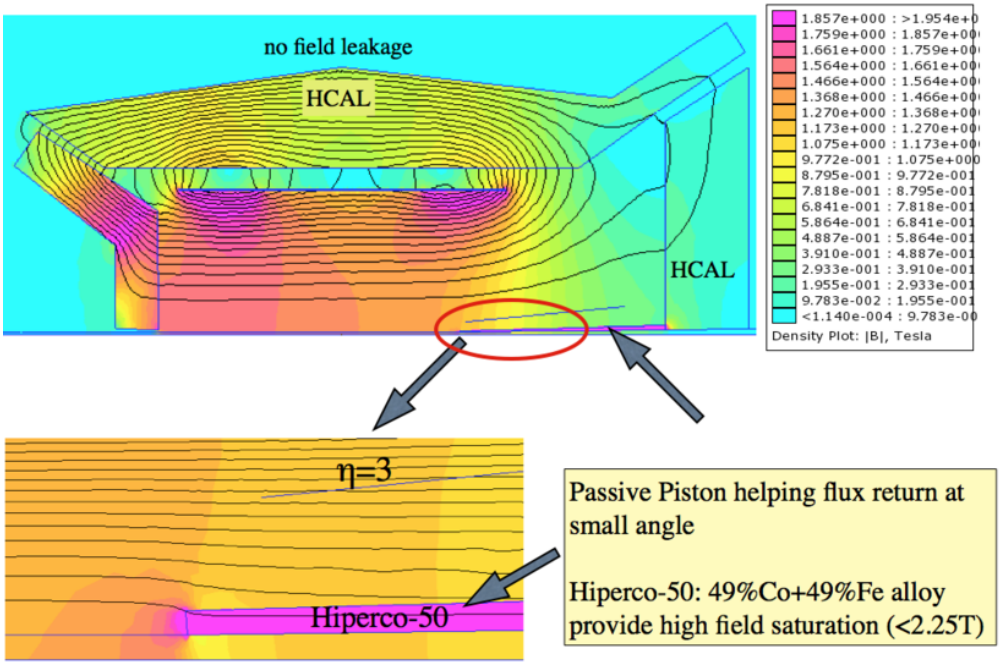

Figure 2.3: Magnetic field configuration. The contour lines represent magnetic field potential as calculated using the 2D magnetic field solver FEMM 2D and Poisson. HCal is assumed to be made of stainless steel and serves as a flux return. Bottom: magnetic field distortion by piston field shaper.

The magnetic piston produces an additional background from particles with $\eta > 4.2$ showering into the piston material. Their contribution is included in the occupancy and performance studies for the baseline detector. Furthermore, this background may be reduced with the addition of tungsten saw-tooth ring shield surrounding the piston. A sketch of this concept is shown in Figure 2.2. With further optimization, these tungsten structures would absorb the particle shower from the interior of the piston, while minimizing inducing additional showers. This solution was previously used in E605 Fermilab experiment [44].

2.3 Tracking Systems

The tracking system provides precise measurements of charged particle momentum and charged hadron angular distribution within jets. It utilizes the combination of a recon-

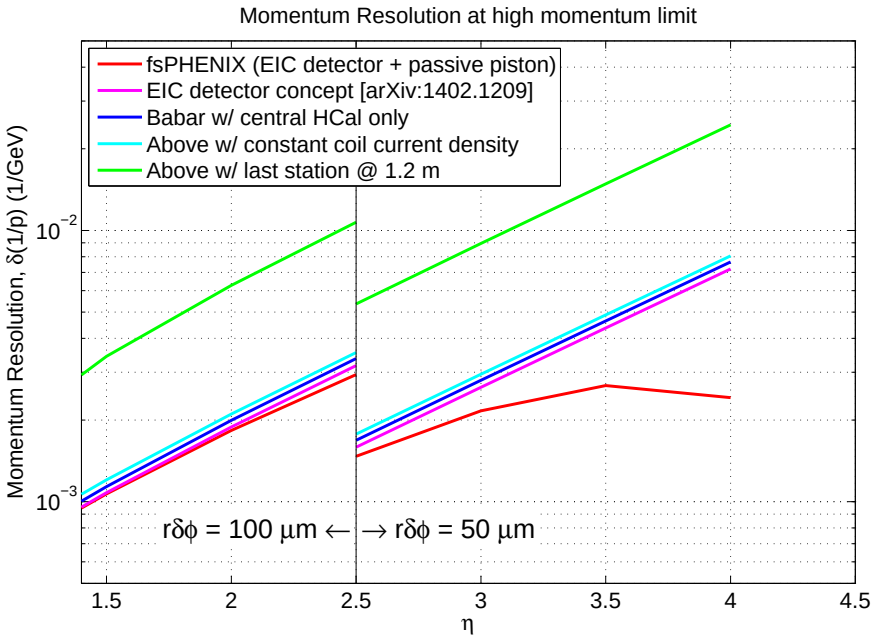

Figure 2.4: Momentum resolution as a function of pseudo-rapidity for different configurations in the high momentum limit. The fsPHENIX tracking resolution is highlighted in red.

figured PHENIX Forward Vertex (FVTX) silicon detector for tracking near the collision vertex, and three GEM planes for intermediate tracking.

2.3.1 Vertex Tracker

The current FVTX has high radial segmentation to measure distance of closest approach of heavy flavor decays in the forward direction. It has nearly 92 ϕ segments formed by wedges with two columns of strips. The current FVTX wedges is going to be re-stacked to obtain high azimuthal segmentation (Figure 2.5). They will form 6 planes in order to cover a broad collision vertex and pseudo-rapidity. The position, dimension and number of wedges in each stations are listed below

disk placement	radius [cm]	number of wedges
20cm	$2.5 < r < 12.1$	48 large, 16 small
25cm	$3.0 < r < 16.0$	64 large, 16 small
30cm	$3.5 < r < 19.5$	80 large, 16 small
60cm	$2.0 < r < 8.0$	32 large, 16 small
65cm	$2.0 < r < 8.0$	32 large, 16 small
70cm	$2.0 < r < 8.0$	32 large, 16 small
TOTAL		288 large, 96 small

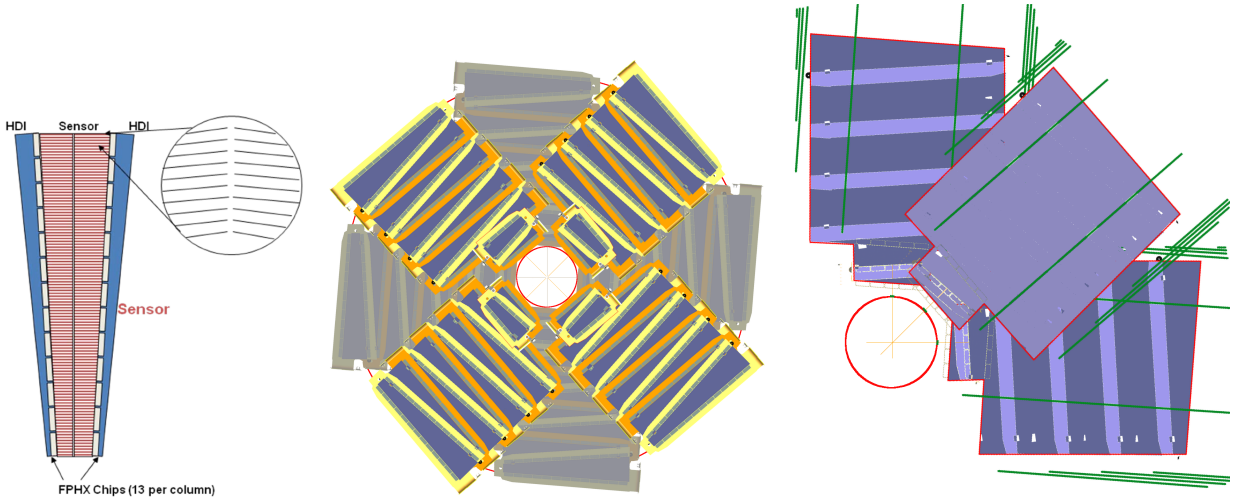

Figure 2.5: Re-stacking of the current FVTX silicon detector. (left) All paddles in one disk. (right) Detail of the active area of the detector showing no holes in acceptance at small angles. Green lines are the extension cables. Red circle corresponds to 3cm radius.

The number of wedges used in the current FVTX in north and south is enough for this re-stacking.

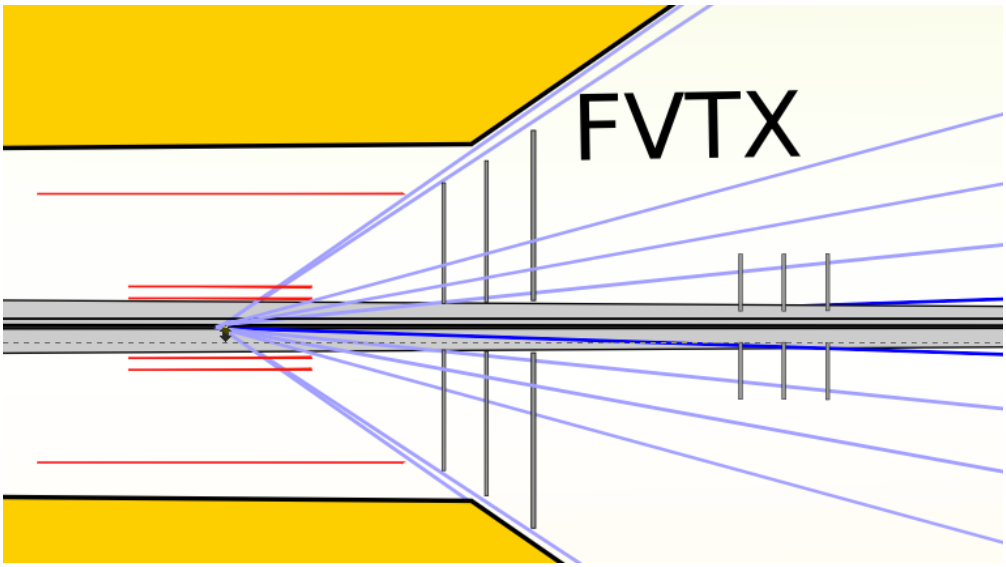

Figure 2.6: Arrangement of the re-stacked FVTX disks.

2.3.2 Intermediate GEM Tracker

The intermediate tracker utilizes three GEM stations at $z = 150$, 200 and 300 cm, covering $\eta = 1$–4. Two last stations sandwich the future RICH detector. The first station locates

at maximal sagitta, the deviation from the track straight line between two other points defined by vertex tracker and GEM station at $z = 300$ cm.

Producing such large area GEM foils (5–20 m^2) is currently a challenging task. However, this technology is under active development at CERN. The single mask etching technology has already allowed fabrication of 2×0.5 m^2 GEMs, which is compatible with fsPHENIX needs.

The readout planes for these devices are optimized to preserve high position resolution in the azimuthal direction $r\delta\phi \sim 50 - 100$ μm and $\sim 1 - 10$ cm in δr, while minimizing the number of readout channels. Here we assume that using mini-drift GEM technology, currently under development [45], 2 mm (1 mm) wide chevron-type readout will provide a $r\delta\phi \sim 100\mu$m (50μm) azimuthal position resolution for the pseudorapidity region $1 < \eta < 2.5$ ($\eta > 2.5$), with minimal material budget. Segmentation in radial direction is defined by particle occupancy within a jet and by precision for hadron azimuthal and polar angle measurements relative to jet axis. For the latter, the readout radial segmentation along with fine azimuthal segmentation will give sub-dominant contribution to the precision of charged hadron measurements relative to jet axis, compared to jet axis precision determination with HCal.

The rate and occupancy of the GEM trackers were studied with full event simulations with the Pythia 6.4 event generator and a GEANT4 detector model. The average hit density for each of the PYTHIA Tune-A hard collision is shown in Figure 2.7.

Folded with the projected $p+p$ collision rate, the GEM rate capability of 100 MHz/cm^2 as demonstrated in the COMPASS experiment [46], is converted to the hit density limit as high lighted by the top horizontal line on each panel. Therefore, the fsPHENIX GEM rate is at least two and one orders of magnitude lower then this limit, for $\sqrt{s} = 200$ GeV and $\sqrt{s} = 510$ GeV proton-proton collisions, respectively.

We further consider channel occupancy for 0.1×1 cm^2 inner GEM strips (used for $4.0 > \eta > 2.5$ region) in rare event trigger with consideration of the multi-collision pile-up. The hit density per collision which would lead to 1% occupancy for a full event is highlighted by the lower horizontal lines on both panels. Comparing this line with the highest end for the GEM hit density curves, we conclude the max occupancies for the GEM trackers are sub-percent and few percent for $\sqrt{s} = 200$ GeV and $\sqrt{s} = 510$ GeV proton-proton collisions, respectively. The current PHENIX FVTX detector demonstrated that pattern recognition for forward tracks can maintain high efficiency at a few-percent channel occupancy level.

Based on simulations, we expect both the GEM rate and occupancy can be further improved by optimizing the shape and density for the tungsten shield rings on the piston yoke (Figure 2.2).

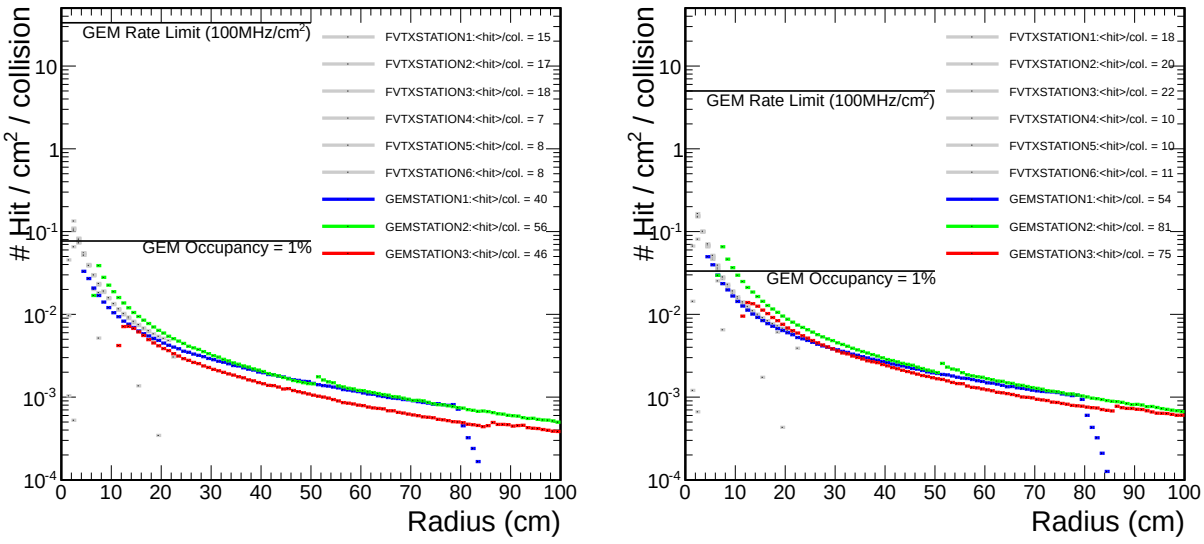

(a) 200 GeV p+p collisions

(b) 510 GeV p+p collisions

Figure 2.7: Hit density on the tracking detectors for each hard proton-proton collision of (a) $\sqrt{s} = 200$ GeV and (b) $\sqrt{s} = 510$ GeV from a GEANT4 simulation. The hit density is proportional to rate and occupancy on the detector. With consideration of projected multiple collision rate, two vertical scales are highlighted with horizontal black lines: GEM rate capability of 100 MHz/cm^2 [46] and 1% channel occupancy for the 0.1×1 cm^2 inner GEM readout strips.

2.4 Hadron Calorimeter

The hadron calorimeter consists of a steel-scintillating tile design with wavelength shifting fiber readout, similar to the central sPHENIX hadron calorimeter with energy resolution better than $100\%/\sqrt{E}$. It will be ~ 5 L_{abs} thick and cover a rapidity range from $1 < \eta < 5$. The steel in the absorber will also serve as part of the flux return for the solenoid magnet. The segmentation will be ~ 10 cm $\times$ 10 cm, resulting in ~ 3000 towers. The readout will use SiPMs, similar to the central sPHENIX calorimeters, which will provide an advantage in being able to use a common readout for all of the calorimeter systems. The same design is suggested for evolution to an EIC detector proposal [2].

The occupancy for the hadron calorimeter is also studied with full event simulations using Pythia 6.4 event generator and a GEANT4 detector model. The occupancy is quantified by the probability that a muon track from a Drell-Yan event can be identified using the cut of HCal scintillator energy < 200 MeV (corresponding to 99% efficiencies for single muons alone). Considering the typical muon energy deposition in HCal is MIP energy (˜50 MeV), this cut roughly requires that the total scintillator energy deposition from the under lying event is smaller than 150 MeV per tower. In this study, we also considered one

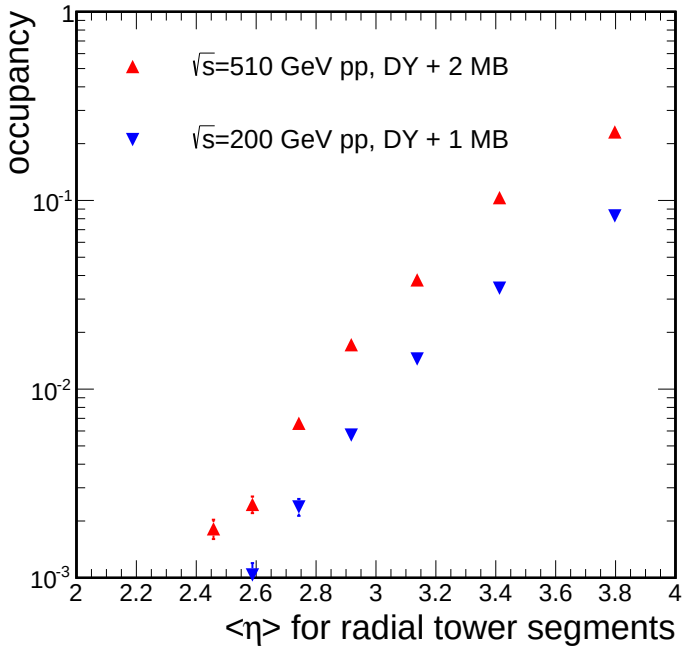

Figure 2.8: Occupancy for the hadron calorimeter, which is quantified by the probability for lying event of Drell-Yan plus multiple-collisions to contribute more than 150 MeV in the scintillator. The $\sqrt{s} = 510$ GeV Drell-Yan production which is piled up with two MB collisions is shown in the red points; the $\sqrt{s} = 200$ GeV Drell-Yan production which is piled up with one MB collisions is shown in the blue points.

and two additional MB collisions per RHIC crossing for $\sqrt{s} = 200$ GeV and $\sqrt{s} = 510$ GeV proton-proton collisions, respectively. The result, as in Figure 2.8, shows the occupancy for $\eta < 3$ is very low at two percent level or less. Between $3 < \eta < 4$, the occupancy is less than 10% and 25% for $\sqrt{s} = 200$ GeV and $\sqrt{s} = 510$ GeV proton-proton collisions, respectively. This occupancy is included in the Drell-Yan projections.

2.5 Muon Identifier

PHENIX North MuID system is used for muon identification in this proposal. It consists of five steel absorber plates interleaved with Iarocci tubes. Multiple layer configuration provides measurements of the trajectory in the MuID. The MuID contributes to the first level trigger decision. For example, muon trigger requires signal in three layers including the last one. The total thickness of absorber plates is $5.4L_{abs}$. HCal ~ 5 L_{abs} thick downstream the MuID provides additional hadron suppression in muon measurements.

We propose to extend the pseudo-rapidity coverage of the PHENIX MuID system from

$\eta = 2.4$ to $\eta = 4$, by building a miniMuID with a design similar to the existing PHENIX MuID. Additional cost savings may be possible by salvaging part of the south Muon Identifier, which is planned to be removed as part of the sPHENIX installation, to construct the miniMuID.

2.6 Possible Hadron PID

While not a part of the baseline fsPHENIX design, the installation of the gas RICH designed for the EIC detector would allow pion (kaon) identification from momenta $\sim$4 GeV/c ($\sim$15 GeV/c) up to $\sim$60 GeV/c in the pseudorapidity range $1 < \eta < 4$ [2]. The gas-based RICH uses CF_4 as a Cerenkov radiator, with the Cerenkov photons focused to an approximately flat focal plane using spherical mirrors of 2 m radius. The photon detector consists of CsI-coated GEM detectors placed at the focal plane. This design is currently funded as an EIC R&D project.

Chapter 3

Physics Performance

In this chapter we summarize the anticipated physics performance of the fsPHENIX detector for measurements in polarized $p+p$ and $p+$A collisions at 200 GeV and polarized $p+p$ collisions at 510 GeV. We begin by listing the anticipated running time and integrated luminosity for each colliding system, followed by a detailed description of key measurements involving jets in polarized $p+p$ collisions and $p+$A collisions, and spin polarized Drell-Yan as measured in the dimuon channel.

While we present a set of simulations that outline the capabilities of the proposed fsPHENIX apparatus and the challenges faced by the proposed physics program, we recognize that much more extensive studies will be required to develop the detector concept to the point where the capability to make the measurements of interest is fully demonstrated.

3.1 Luminosity and Running Time Assumptions

In this section we list the assumptions regarding running time and integrated luminosity that are integrated into the descriptions of the physics performance that follows in later sections.

The charge from BNL Associate Lab Director Berndt Mueller tasked us to consider polarized $p+p$ and $p+$Au running in the time period RHIC FY 2021–2022 (see Appendix A for the complete charge). The charge specifies delivered luminosities from RHIC as $200 pb^{-1}$/week for $p+p$ collisions at 510 GeV, and $300 nb^{-1}$ for $p+$Au collisions. No guidance is given for 200 GeV $p+p$ collisions, and the charge cautions that "Since these numbers represent substantial increases over historically achieved luminosities, it may be prudent to assume somewhat lower numbers for estimates of required beam times."

Additional guidance for anticipated RHIC luminosity can be found in the RHIC Collider Projections document [47], which projects minimum and maximum collider luminosity and polarization performance for 2014–2018. The projections for the CAD delivered luminosity

per week in the document are consistent with the ALD guidance, while the minimum luminosity is consistent with the Run-12 and Run-13 achieved values for 200 GeV and 510 GeV p+p. As a conservative estimate, we have chosen to average the maximum and minimum values from [47] for the delivered luminosity when calculating the statistical power of measurements. This leads to the following CAD delivered luminosity values:

- For 200 GeV p+p, 18.7pb^{-1}/week
- For 510 GeV p+p, 128pb^{-1}/week
- For 200 GeV p+A, 225nb^{-1}/week (p+p equivalent luminosity of 44pb^{-1}/week)

For polarization we assume 60% beam polarization in p+p and p+Au collisions, consistent with historically achieved values. We note that CAD guidance projects that polarizations up to 70% may be possible.

The sampled luminosity will depend on the PHENIX uptime and the vertex cut. For the PHENIX uptime we use the achieved value of 0.6. The vertex cut applied depends on the analysis. For jet observables we assume a vertex cut of $\pm$30cm and an efficiency of 0.87, consistent with a vertex distribution in the PHENIX interaction region with $\sigma = 20$cm. For Drell-Yan dimuon pairs an asymmetric vertex cut of $-30 < z_{VTX} < 10$cm is used to take optimal advantage of the delivered luminosity, consistent with the use of the FVTX to eliminate heavy flavor backgrounds. Such an asymmetric vertex cut implies an acceptance that varies as a function of vertex position. This effect is folded into the tracking efficiency when estimating statistics for the DY program, as described in a later section.

During RHIC FY 2021–2022 we assume one 10-week running period of 200 GeV polarized p+p collisions, and one 10-week running period of 200 GeV p+Au collisions. These running periods will be required to provide reference data for the sPHENIX Heavy Ion program and are consistent with the proposed sPHENIX run plan [1]. In addition, we also list integrated and sampled luminosity for one potential 15-week running period at 510 GeV for a dedicated Drell-Yan physics run. The delivered and sampled luminosity is summarized in Table 3.1.

System	Run Length	CAD Delivered Luminosity (pb^{-1})	Sampled Lumi. Jets (pb^{-1})	Sampled Lumi. Drell-Yan (pb^{-1})
p+p (200 GeV)	10 weeks	187	97	69
p+Au (200 GeV)	10 weeks	440 (p+p equiv)	230 (p+p equiv)	164 (p+p equiv)
p+p (510 GeV)	15 weeks	1,280	1002	714

Table 3.1: CAD delivered and fsPHENIX sampled luminosity for Jets and Drell-Yan as a function of collision system.

For the jet measurements, we assume a 20kHz sPHENIX/fsPHENIX DAQ event rate, with 10kHz allocated to fsPHENIX, and 5kHz of that allocated to jet physics. The performance

plots in the following sections assume an HCAL-based jet trigger that is prescaled at lower energies to keep the combined jet trigger rate below 5kHz, see Table 3.2. The statistics used the the jet performance plots in the following sections take into account the prescale factors when calculating the statistics in each bin.

Jet Energy (GeV)	Rate (kHz)	Prescale	DAQ Rate (kHz)
$10 < E < 20$	12.44	7	1.56 kHz
$10 < E < 30$	9.05	4	1.81 kHz
$30 < E < 50$	4.14	2	1.31 kHz
$50 < E < 100$	0.31	0	0.31 kHz

Table 3.2: Jet rates and assumed prescale factors for 200 GeV running, assuming the CAD average luminosity from [47]. The corresponding minimum bias interaction rate is 3.2MHz.

For the Drell-Yan measurements, we assume the development of a MuID-based dimuon trigger with high rejection capable of using the full luminosity sample in 3.1. Such a trigger is a feasible extension of the existing MuID trigger extended to use individual MuID panels to reduce combinatorics that limit the rejection power of the existing trigger.

3.2 Jet Measurements with fsPHENIX

The initial fsPHENIX performance for jet related measurements have been studied with a parameterized fast simulation based on initial GEANT4 simulations of the fsPHENIX detector including the modified FVTX detector, three GEM layers and the forward hadronic calorimeter. The event sample was created using Pythia 6.4 with TuneA and no further modifications to the intrinsic transverse momentum. Jets were identified in the rapidity range 1.7 to 3.3 with an anti-kt algorithm of cone size 0.7 to allow the full jet to be contained within the forward detector acceptance of 1 to 4.

The jet energy resolution will driven by the hadronic response with the calorimeter and so is expected to be approximately $100\%/\sqrt{E}$ or better. Optimizations to the hadronic calorimeter design, such as longitudinal segmentation, may be required to limit the impact of shower leakage and are being considered. A full estimation of the jet energy resolution awaits a complete GEANT4 study and will be an immediate focus of future effort.

However, one specific concern raised in use of forward jet reconstructions for the Collins physics extraction was the impact of the jet 4-vector angular resolution. If a large discrepancy between the reconstructed jet center via the energy deposit in the calorimeter and the fragmentation measured via the track would wash out the Collins physics signal. This resolution was modeled with the fast simulation using an HCAL with 5 cm x 5 cm towers and a model of electromagnetic and hadronic showers including fluctuations. In the far forward region $\eta = 3 - 4$, jet angular resolutions at large energy within this model were found to be $\Delta\eta \sim 0.05$ and $\Delta\phi \sim 0.05 rad$. For jets reconstructed at $\eta = 1 - 2$, the pointing

resolutions at large jet energy improve to $\Delta\eta \sim 0.02$ and $\Delta\phi \sim 0.02rad$. A follow up study using the full GEANT4 simulation is still needed and will be performed to confirm these results with a fleshed out HCAL design, but the results from this initial study are characteristically small and should not adversely impact the Collins physics program.

3.2.1 Jet Asymmetries

As described in Section 1.1, the measurement of the inclusive jet single spin asymmetry accesses the correlation between the spin of the proton and transverse motion of its partonic constituents. The fsPHENIX jet measurements will be the first real jet asymmetries at $\sqrt{s} = 200$ GeV, but given the weak energy dependence seen for the pion single spin asymmetries [48] a comparison to existing AnDY results at 500 GeV is useful. The size of the expected inclusive asymmetry in recent theoretical calculations by [17] as a function of the reconstructed x_F of the jet for transverse momenta above 4 GeV/c is shown in Figure 3.1. As shown in the right panel, the authors achieve the small asymmetry in the AnDY jet measurement with a substantial cancellation between jets arising from up and down quarks.

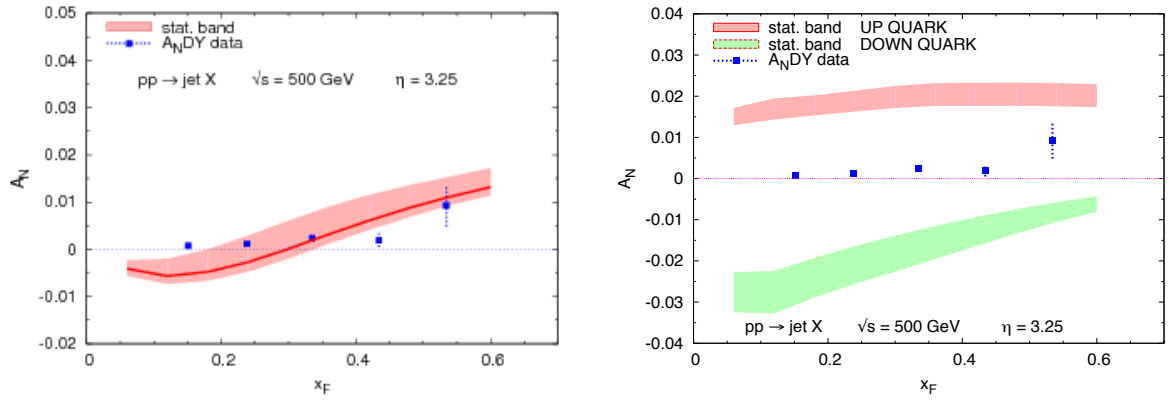

Figure 3.1: AnDY single spin asymmetries together with the best parameterization based on the Sivers function from SIDIS displayed separately for jets originating from u and d quarks (bottom) and combined(top).

Both Anselmino, et al. and Gamberg, Kang, & Prokudin have provided us with estimations for the jet single spin asymmetry $\sqrt{s} = 200$ GeV for $\eta = 2.5$, a value in the center of our acceptance. These are shown in Figure 3.2 along with an estimation of the statistical precision achievable with fsPHENIX in a baseline year of 97 pb^{-1}. Since the cancelation needed for the AnDY result is different between the models, the predictions for fsPHENIX vary. Thus a measurement of inclusive jets in the forward direction at $\sqrt{s} = 200$ GeV begin to test these models. Furthermore, the open design of fsPHENIX will also allow subsets within η to be studied separately, allowing multiple tests of this kind, something that was not possible within the more narrow acceptance of AnDY.

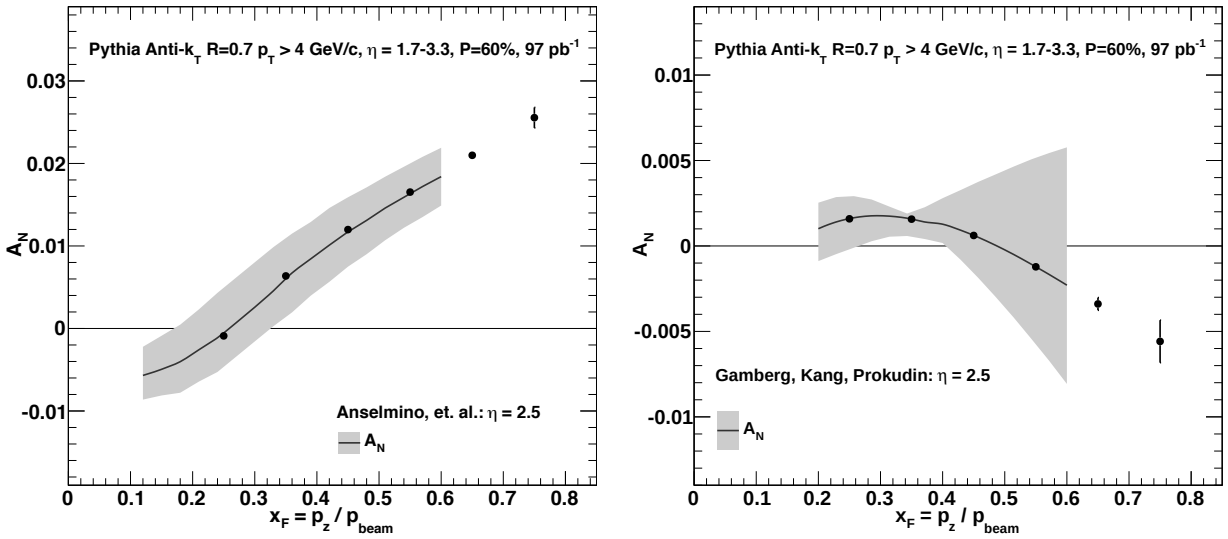

Figure 3.2: Projected statistical precision for jet A_N measurements for model predictions from Anselmino, et. al. (left) and Gamberg, Kang, & Prokudin (right) using jets with $p_T > 4$ GeV/c in the pseudorapidity range 1.7–3.3. Shaded bands depict existing theoretical uncertainties assuming a fit to world data involves no spin-dependent fragmentation. Bars show the expected statistical uncertainties from 97 pb^{-1} of p+p at 200 GeV.

The more interesting question is whether the partial cancellation of the contribution of up and down quarks responsible for the small size of the inclusive jet asymmetries can be measured experimentally. By selecting jets with positively charged hadrons or negatively charged hadrons with fractional energies $z > 0.5$ one can bias the jet's partonic process fractions towards larger up or down quark fractions. Based on the parton information from Pythia simulations, one can find that this selection improves the u quark purity at large z to 80% and the d quark purity to 30% of all jets, see Fig. 3.3. Under the positive charge sign requirement, the up quark contribution reaches high purities easily across all of the inspected x_F values. The down quark contribution is enhanced over the natural abundance by nearly a factor 3 in the negatively charged leading hadron sample, but does not rise above the up quark fraction for two reasons: (1) the smaller initial fraction provided by nature and (2) a weaker response to the charge sign requirement due to the down quark's smaller 1/3 electrical charge.

Jets in the acceptance will also arise from other sources, namely gluons but also a smaller portion from proton beam remnants in the forward-most parts of the detector. These other sources are small at large x_F, contributing below 20% to the jet sample. At smaller x_F the contribution from gluons rises as should be expected from changes in the parton distribution function. Beam remnants have been simulated using a PYTHIA $k_T = 0.36$ GeV/c setting appropriate for fragmentation scale processes and matching BRAHMS proton/pion ratios at forward rapidity. Other contributions were calculated using hard scattering settings within Tune A.

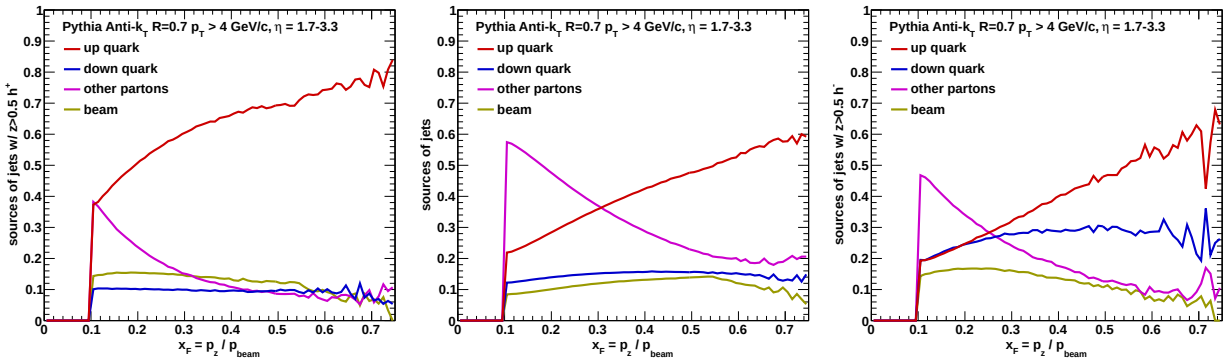

Figure 3.3: Up (red), down (blue) quark and other purities (magenta and brown) for jets in the rapidity range 1.7–3.3 and transverse momenta above 4 GeV as a function of the reconstructed jet x_F when requiring a h^+ (left figure) with $z > 0.5$, or no hadron selection (middle figure), or h^- (right figure) with $z > 0.5$.

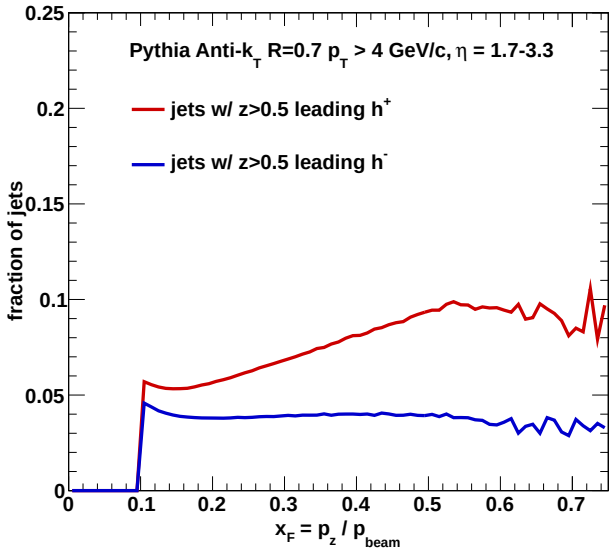

Figure 3.4: Positive leading charge cut efficiency (red) and Negative leading charge cut efficiency (blue) for jets with $p_T > 4$ GeV/c in the pseudorapidity range 1.7–3.3.

The charge sign selection cuts needed to enrich quark fractions away from the natural abundance will reduce the statistical sample of jets that are analyzed as only a portion of the fragmentations will produce leading charged hadrons. These efficiencies are shown in Fig. 3.4 for both the leading positive charge cut and the leading negative charge cut. The efficiency for the positive charge selections rises from 6% at low x_F to 10% at large x_F, a reflection of the rapidly increasing up quark contribution to the parton distribution function. The efficiency for the negative charge sign selection remains at a level 4% across x_F.

Deeper inspection of the jet fragmentation will gather more information than the examination of the leading particle only and will allow the construction of more sophisticated cuts

for creating up and down quark enrichment while preserving more of the jets sample for analysis. These very simple cuts are sufficient for extracting the key jet spin asymmetries and leave further improvements of optimization to future work.

We now evaluate our ability to extract up and down quark spin asymmetries using a simple illustrative model comprised of the jet purities shown in Fig. 3.3, the efficiencies of our jet charge sign cuts shown in Fig. 3.4, and two models proposed of the up and down quark canceling needed to reproduce the inclusive jet spin asymmetries measured by AnDY with the jet statistics collected in a baseline year of p+p collisions with an integrated luminosity of 97 pb^{-1}. An examination of the unfolding of the jet energy resolution is not considered but will be examined in future work. The results of these two evaluations are shown in Fig. 3.5. The theoretical inputs are taken from the bands and linearly extrapolated to cover the full x_F range. The A_N values for up and down quarks are applied for the jet fractions within the positive charge selected, the natural abundance, and the negative charge selected sample separately. Other sources of jets were taken to contribute no asymmetry. The beam polarization was taken to be 60%. The resulting raw measurement projections are shown in the left column of Fig. 3.5. Statistical uncertainties are applied to these projections after accounting is made for the efficiencies of the leading charge cuts. The uncertainties are larger for the negatively charged hadron cuts where the efficiencies are lower. The inclusive jet sample is corrected for the beam polarization and appears in the final form in the right column. A simple two parameter fit is applied to the three raw measurements with our model of the jet purities to extract the projected statistical uncertainties on the theoretical inputs, also shown in the right column. The precision on the up and down quark A_N is similar after extraction as all three inputs from the left column were used.

The results of this illustrative example demonstrate how the sign of the A_N cancellation in the inclusive jet sample will be immediately apparent already in the raw measurements. Our final ability to distinguish between the up and down quark contributions to the inclusive A_N will depend on how large that cancellation is in nature. The two theoretical descriptions have different scales for this cancellation, but both are readily distinguished by the expected statistical precision of the jet sample to be collected. In both cases, the statistical precision will improve on the theoretical model uncertainty from fitting other world data.

3.2.2 Collins Asymmetries

For the Collins asymmetries the same jets were selected as in the previous subsection. In addition charged hadrons were selected in these jets and their fractional energies $z = E_h / E_{jet}$ were calculated. The azimuthal asymmetries were then evaluated as a function of z as shown in Figures 3.6 and 3.7, where the resolution in z (dominated by the energy resolution of the HCAL) is included in the binning shown in the Figures. One can see that very good precision out to relatively large z can be reached.

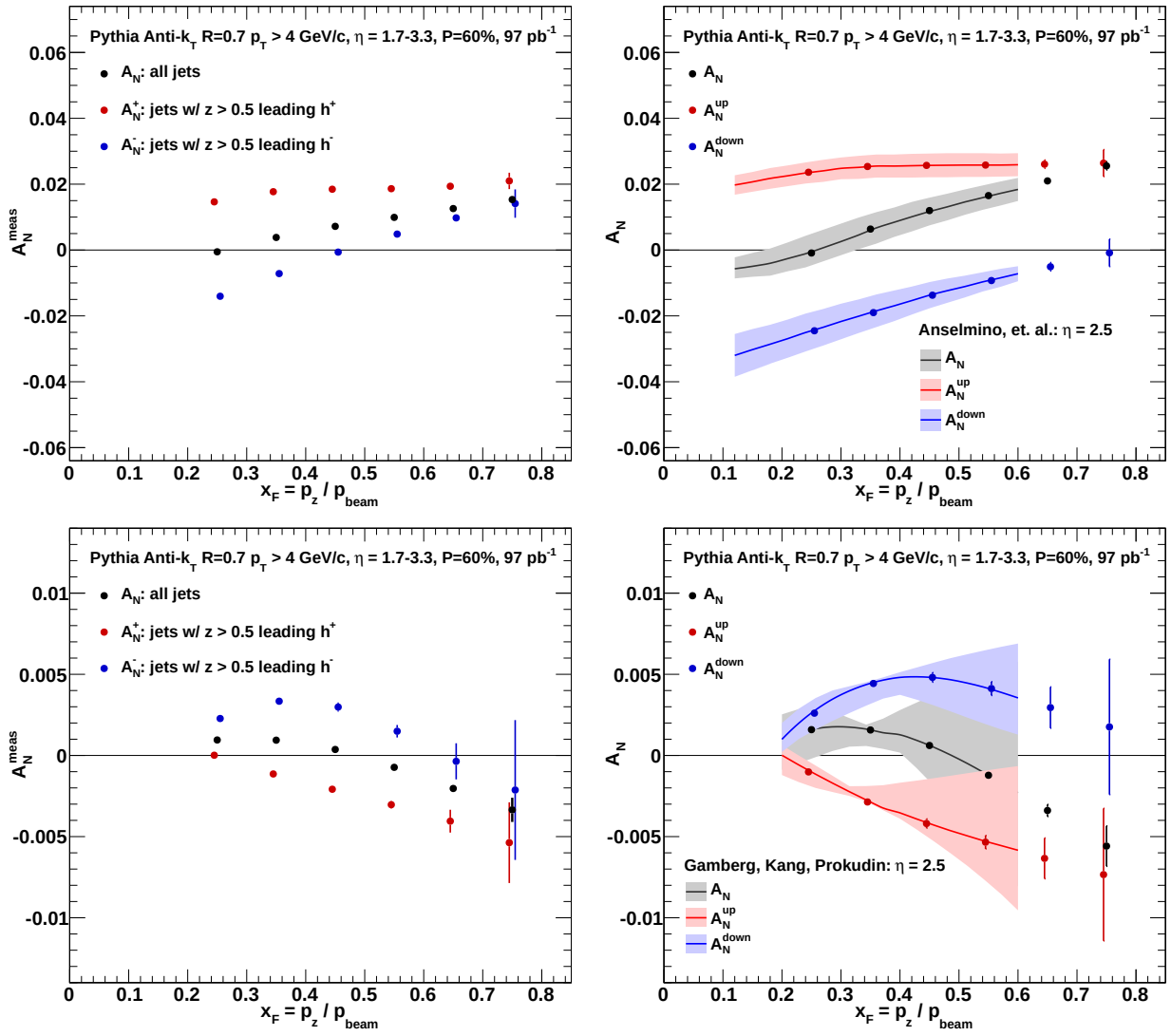

Figure 3.5: Projected statistical precision for jet A_N measurements (left column) and extracted theory constraints (right column) for theoretical inputs from Anselmino, et. al. (top row) and Gamberg, Kang, & Prokudin (bottom row) using jets with $p_T > 4$ GeV/c in the pseudorapidity range 1.7–3.3. Shaded bands depict existing theoretical uncertainties assuming a fit to world data involves no spin-dependent fragmentation. Bars show the expected statistical uncertainties from 97 pb^{-1} of p+p at 200 GeV.

For the selected data x ranges can be probed above the previously available SIDIS measurements of about 0.3. The ranges probed as function of jet energy bin are displayed in Fig. 3.8 where one can see, that the higher jet energies at the forward rapidities generally reach x of 0.5 to 0.6 at $\sqrt{s} = 200$ GeV. This will allow to better constrain the global transvsersity analysis and provide the full range of integration for the up and down tensor charges of the nucleon.

If the baseline fsPHENIX detector were extended with full pion-kaon particle identification

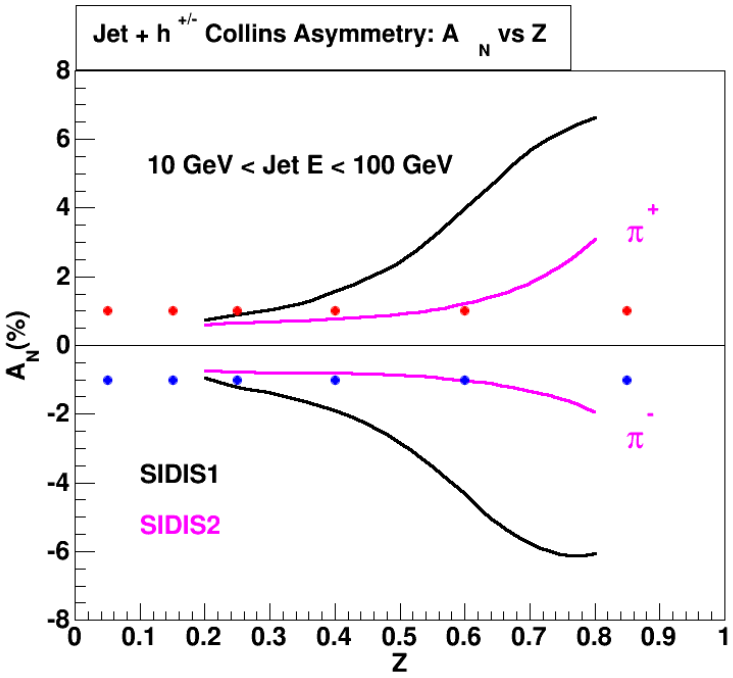

Figure 3.6: Expected single spin asymmetry $A_N^{\sin(\phi-\phi_h)}$ sensitivities for charged hadrons in jets in the rapidity range 1.7–3.3 and transverse momenta above 4 GeV as a function of the fractional hadron energy z for h^+ (red points) or h^- (blue points). The expected asymmetries for pions based on the SIDIS Collins fits are also displayed. The error bars shown are statistical only.

capabilities, for example with the RICH planned for the EIC detector [2], one could also extract pion and kaon asymmetries separately. This would allow a full flavor decomposition of the transversity distribution into at least up, down and sea quarks or possible even distinguishing the light and strange sea. The corresponding kaon Collins fragmentation functions are expected to be obtained in the Belle experiment well in advance of the fsPHENIX era. The expected uncertainties on the kaons asymmetries are shown in Figure 3.9. A gas RICH detector is assumed for charged kaon identification in the momentum range of 15–60 GeV. Even with the substantially smaller unpolarized kaon fragmentation functions for light quarks and the rapidly falling spectrum of light hadron fragmentation functions good statistics are available when integrated over the full jet energy range.

3.3 Drell-Yan Measurements with fsPHENIX

One of the goals of fsPHENIX is to investigate the Sivers transverse-spin asymmetry in the Drell-Yan process in order to compare it with that from the DIS process and to test the "non-universality". This has become one of the top priorities for the world-wide hadronic physics community. We need to measure the asymmetry in the Drell-Yan process to collect

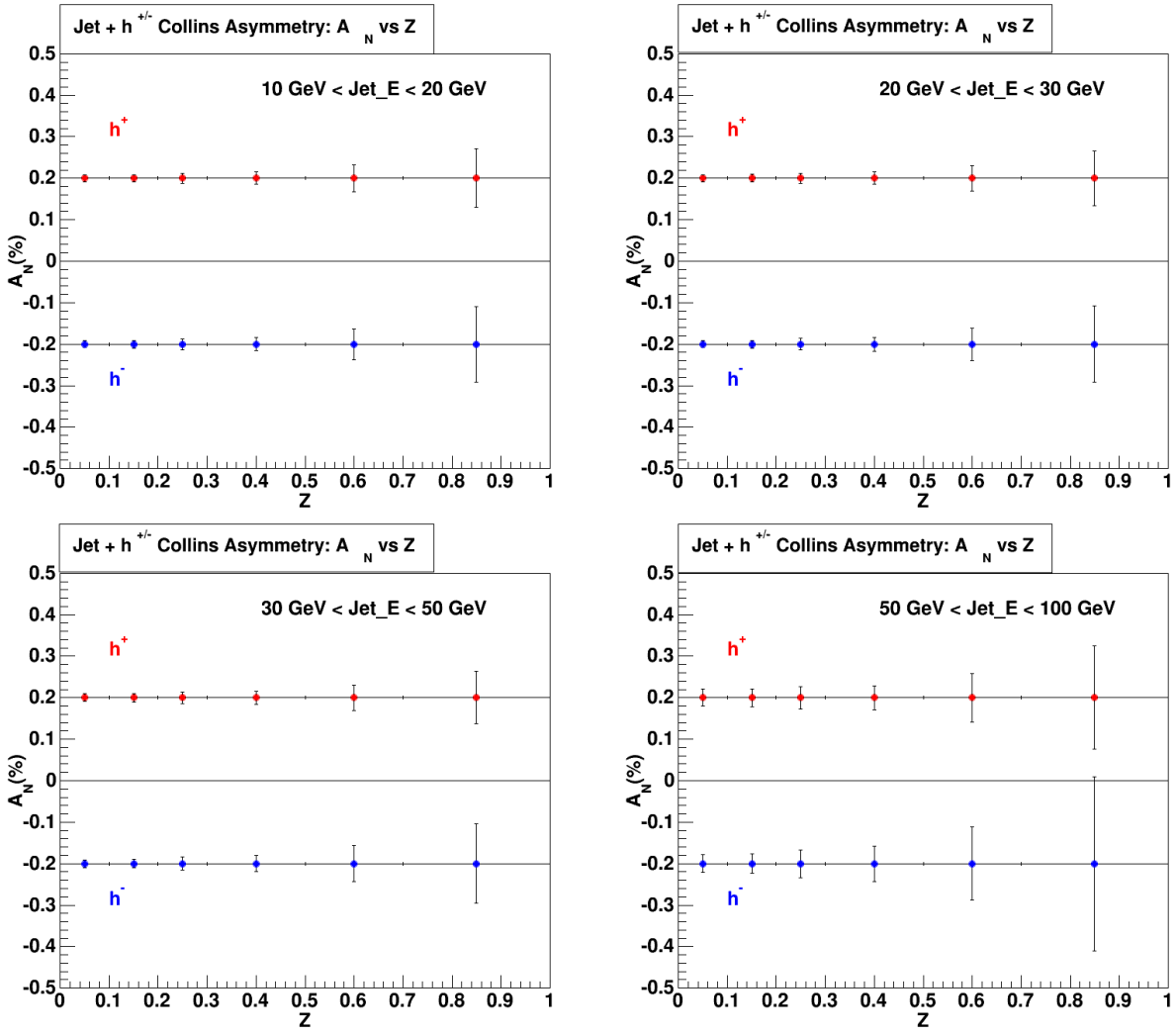

Figure 3.7: Expected single spin asymmetry $A_N^{\sin(\phi-\phi_h)}$ sensitivities for charged hadrons in jets in the rapidity range 1.7–3.3 and transverse momenta above 4 GeV as a function of the fractional hadron energy z for h^+ (red points) or h^- (blue points), for different jet energy ranges. The error bars shown are statistical only.

a significant amount of statistics to be comparable with that of the DIS data.

The polarized Drell-Yan measurement is a competitive program in fixed-target experiments and in collider experiments. A comparison of the asymmetries at fixed-target energies and collider energies also provides a unique test of TMD evolution.

Table 3.3 shows a comparison of the polarized Drell-Yan measurement in COMPASS-II and fsPHENIX. Information on COMPASS-II is obtained from the COMPASS-II proposal [49]. In order to compare the kinematic coverage and statistics by COMPASS-II and fsPHENIX, we performed a simple PYTHIA simulation on Drell-Yan signal with simple geometrical acceptance without magnetic field. For COMPASS-II, we assumed a detector acceptance

	COMPASS-II	fsPHENIX 200 GeV	fsPHENIX 510 GeV
$L_{avg}(\mathrm{cm}^{-2}\mathrm{s}^{-1})$	1.18×10^{32}	0.76×10^{32}	6.48×10^{32}
Average L /week	14.3 pb^{-1}/week	18.7 pb^{-1}/week	128 pb^{-1}/week
Accelerator eff.	0.8	(included above)	(included above)
Detector up-time	0.85	0.6	0.6
Vertex cut	n/a	0.62	0.62
Sampled L /week	9.7 pb^{-1}/week	6.9 pb^{-1}/week	47.6 pb^{-1}/week
week/year	20	10	15
Sampled L /year	194 pb^{-1}/year	69 pb^{-1}/year	714 pb^{-1}/year
Dimuon trigger eff.	0.81	0.81	0.81
High mass: 4 GeV/c^2 < M < 9 GeV/c^2			
Reconstruction eff.	0.8	0.312	0.305
Offline L /year	126 pb^{-1}/year	17.5 pb^{-1}/year	177 pb^{-1}/year
Cross section σ	1291 pb	1199 pb	2542 pb
Acceptance Ω	0.35	0.14	0.19
$\sigma\cdot\Omega$	452 pb	171 pb	478 pb
K factor (assumption)	2	1.38	1.38
Dimuon/year $L\cdot\sigma\cdot\Omega\cdot K$	115000/year	4150/year	117000/year
FoM/year	2230/year	747/year	14600/year
$\delta A_T^{\sin\phi_S} = 1/\sqrt{FoM}$	0.021	0.037	0.0083
Low mass: 2 GeV/c^2 < M < 2.5 GeV/c^2			
Reconstruction eff.	0.8	0.285	0.272
Offline L /year	126 pb^{-1}/year	16.0 pb^{-1}/year	157 pb^{-1}/year
Cross section σ	6231 pb	2811 pb	4630pb
Acceptance Ω	0.43	0.22	0.21
$\sigma\cdot\Omega$	2679 pb	610 pb	955 pb
K factor (assumption)	2	1.38	1.38
Dimuon/year $L\cdot\sigma\cdot\Omega\cdot K$	674000/year	13500/year	207000/year
FoM/year	13200/year	2430/year	25900/year
$\delta A_T^{\sin\phi_S} = 1/\sqrt{FoM}$	0.0087	0.020	0.0062

Table 3.3: Comparison of Drell-Yan measurements by COMPASS-II and fsPHENIX ($1.2 < \eta < 4$), where FoM (Figure of Merit) is $N/2\cdot(f\cdot|S_T|)^2$ (COMPASS-II, $f = 0.22$, $|S_T| = 0.9$) or $N/2\cdot P^2$ (fsPHENIX, $P = 0.6$ at $\sqrt{s} = 200$ GeV and $P = 0.5$ at $\sqrt{s} = 510$ GeV).

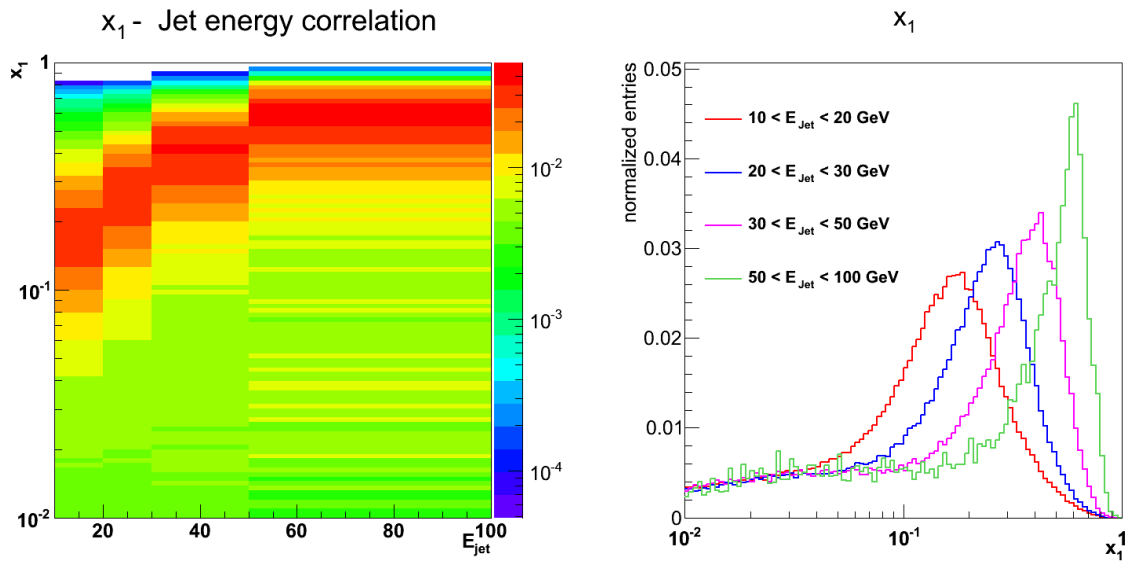

Figure 3.8: x_1 probed by charged hadrons in jets in the rapidity range 1.7–3.3 and transverse momenta above 4 GeV as a function of the jet energy at $\sqrt{s} = 200$ GeV. Left: A 2-dimensional representation of jet energy and x_1 range, normalized by all events per energy bin is displayed; right: Individual x_1 distributions as a function of jet energy bin at $\sqrt{s} = 200$ GeV.

determined by the MW1, and studied with beam momentum of 190 GeV/c. For fsPHENIX, we applied pseudo-rapidity cut $1.2 < \eta < 4$, and studied with collision energies of 200 GeV and 510 GeV. Other factors used to calculate fsPHENIX kinematics and statistics are:

- Detector up-time: 60% is assumed, consistent with PHENIX experience.
- Vertex cut: estimated to be 62% for -30 cm $< v_z <$ 10cm by assuming a Gaussian vertex width of 20 cm.
- Dimuon trigger efficiency: 0.9 for each muon, $0.9^2 = 0.81$ for dimuon pair.
- Reconstruction efficiency: calculated using a GEANT4 model of the fsPHENIX detector and tracking model:
  - muon single-track efficiency:
    - GEM acceptance $\times$ efficiency per plane = 0.9, $0.9^3 = 0.729$ for 3 planes of GEM.
    - MuID efficiency 0.95 per plane, a combined efficiency of 0.999 by requiring 3/5 hit planes.
  - tracking efficiency for dimuon pair: momentum dependence evaluated with GEANT4 tracking simulation.

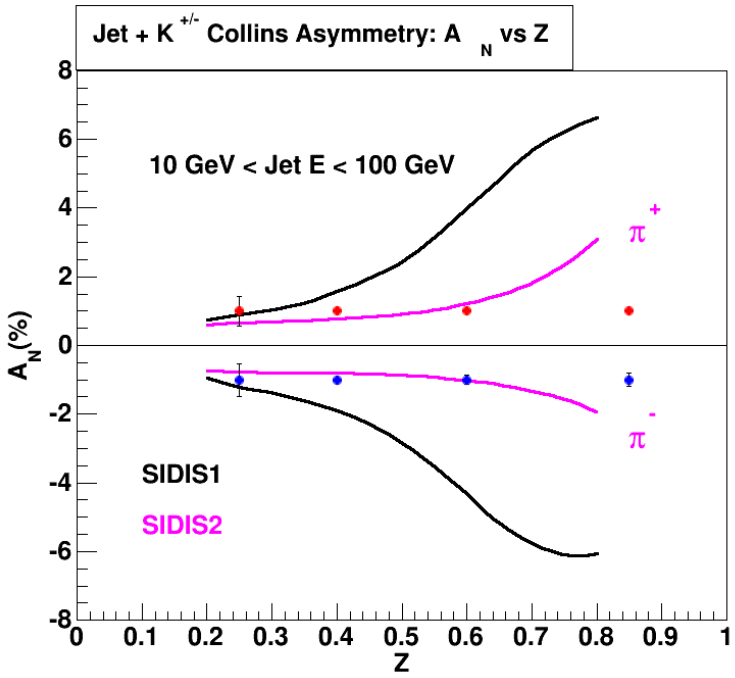

Figure 3.9: Expected single spin asymmetry $A_N^{\sin(\phi-\phi_h)}$ sensitivities for charged kaons in jets in the rapidity range 1.7–3.3 and transverse momenta above 4 GeV as a function of the fractional hadron energy z for K^+ (red points) or K^- (blue points). The expected asymmetries for pions based on the SIDIS Collins fits are also displayed. A gas RICH detector is assumed for charged kaon identification in the momentum range of 15–60 GeV.

– HCAL cut efficiency for dimuon pair: evaluated with GEANT4 HCAL simulation.

Using the efficiencies listed above and the luminosity assumptions listed in Section 3.1 combined with cross section estimates from PYTHIA, we can estimate the total number of Drell-Yan pairs measured by fsPHENIX in different kinematic bins (see Table 3.4. The cross section from PYTHIA were scaled with a k-factor of 1.38, consistent with the scaling between PYTHIA and NLO cross section results.

In order to compare the power of the COMPASS-II and fsPHENIX measurements, a Figure of Merit (FoM) is defined by $N/2 \cdot (f \cdot |S_T|)^2$ ($f = 0.22$, $|S_T| = 0.9$) for COMPASS-II and $N/2 \cdot P^2$ for fsPHENIX ($P = 0.6$ at $\sqrt{s} = 200$ GeV and $P = 0.5$ at $\sqrt{s} = 500$ GeV). The statistical uncertainty of the asymmetry measurements is evaluated by $\delta A_T^{\sin\phi_S} = 1/\sqrt{FoM}$. Figure 3.10 shows a comparison of the FoM for COMPASS-II and fsPHENIX as a function of the partonic x sampled in the proton. At $\sqrt{s} = 200$ GeV, the fsPHENIX measurements has a lower overall FoM but covers higher x than COMPASS-II and it is a complementary measurement. The lower overall FoM could be addressed with additional running time. At $\sqrt{s} = 510$ GeV, fsPHENIX can measure the Drell-Yan A_N with much higher statistics (FoM) than COMPASS-II, with both lower-x and higher-x coverage for $4 < M < 9$ GeV/c^2.

Table 3.4: Estimated number of Drell-Yan pairs assuming 10 week RHIC runs for p+p and p+Au collisions at 200 GeV, and a 15 week run for p+p collisions at 510 GeV

		$2 < M < 2.5\ GeV/c^2$	$4 < M < 8\ GeV/c^2$
200 GeV p+p	$\mathbf{1.2 < y < 4.0}$	13,500	4,200
(10 weeks)	$\mathbf{1.2 < y < 2.0}$	1,900	1,200
	$\mathbf{2.0 < y < 3.0}$	8,000	2,700
	$\mathbf{3.0 < y < 4.0}$	3,200	200
200 GeV p+Au	$\mathbf{1.2 < y < 4.0}$	30,400	4,400
(10 weeks)	$\mathbf{1.2 < y < 2.0}$	4,400	2,800
	$\mathbf{2.0 < y < 3.0}$	18,900	6,500
	$\mathbf{3.0 < y < 4.0}$	7,800	500
510 GeV p+p	$\mathbf{1.2 < y < 4.0}$	207,000	117,000
(15 weeks)	$\mathbf{1.2 < y < 2.0}$	23,300	20,300
	$\mathbf{2.0 < y < 3.0}$	113,400	72,500
	$\mathbf{3.0 < y < 4.0}$	72,500	26,600

Figure 3.11 shows comparison of Drell-Yan kinematics on x_p vs Q^2 between COMPASS-II and fsPHENIX, and also with existing polarized SIDIS data. SIDIS data shown by closed circles exist in the relatively small Q^2 region. Only 2 data points of COMPASS SIDIS overlap with high-mass polarized Drell-Yan plan. For comparison of SIDIS A_N and Drell-Yan A_N in different kinematics region, theoretical calculation of the Q^2 evolution and experimental shape measurement of A_N covering wide kinematic region is important.

Figure 3.12 shows the statistical sensitivities of a Drell-Yan A_N measurement at fsPHENIX, compared with a theoretical calculation of the Drell-Yan A_N without Sivers function evolution [50] and with Sivers function evolution [42].

In order to make asymmetry measurements like those shown in Firgue 3.12, fsPHENIX must be able to separate the Drell-Yan pairs from the substantial backgrounds from heavy flavor and hadrons. Physics background source simulations have been done with PYTHIA at $\sqrt{s} = 200$ GeV and $\sqrt{s} = 510$ GeV. Drell-Yan, open and bound-state heavy-flavor, and light-hadron (QCD jet) events were generated, and all charged tracks in $1.2 < \eta < 4.0$ were used as source of invariant mass calculation of unlike-sign pairs. A GEANT4 simulation of the fsPHENIX detector was used to quantify the rejection and efficiencies of various analysis cuts as well as the overall tracking efficiency for both Drell-Yan pairs and background sources. The MuID and HCAL are used to reject hadrons, while a DCA cut at

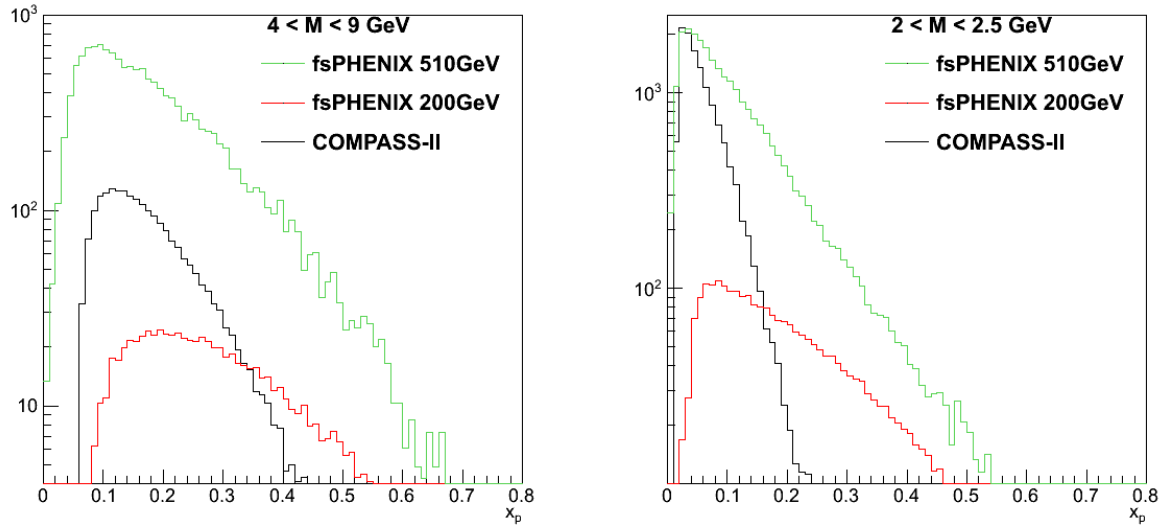

Figure 3.10: Left: A comparison of the FoM of COMPASS-II and fsPHENIX at high mass 4 GeV/c^2 < M < 9 GeV/c^2. The black line shows FoM of COMPASS-II, the red line shows FoM of fsPHENIX at $\sqrt{s}$ = 200 GeV and the green line shows FoM of fsPHENIX at $\sqrt{s}$ = 510 GeV. Right: A similar comparison of FoM of COMPASS-II and fsPHENIX at low mass 2 GeV/c^2 < M < 2.5 GeV/c^2.

1mm is used to to reject π and K as well as some heavy flavor background.

Because the transverse momentum distribution of pairs from background sources is much softer than Drell-Yan pairs (see Figure 3.13), a transverse momentum cut can be very effective in improving the S/B ratio. Because of this, we show the results of the background simulation as a function of a cut on transverse momentum. We do note, however, that a comparison with the SIDIS results and the prediction of modified universality require $q_T < M$, while $q_T > M$ would be the regime in which the higher-twist formalism would be appropriate for interpreting the data. While a q_T cut could be used to improve the S/B ratio at high M, at the expense of statistics, only a modest cut could be used for the low mass region if the results is to be compared with SIDIS.

The DCA resolution is estimated to be of 500 μm with the re-stacked FVTX in p+p collisions. The main limitation is the determination of the primary vertex. A DCA cut at 1mm preserve most of the Drell-Yan yield but has a limited background rejection (Fig. 3.14). Tighter cuts and additional studies to improve DCA resolution with the FVTX can help to increase the signal/backgound for Drell-Yan dimuons all over the mass spectrum.

Figure 3.15 shows the invariant mass of all the unlike-sign pairs from each of generated events at 200 GeV. There is a large background from π-π, π-K, K-K, π-μ, K-μ pairs that must be dealt with, especially at low mass. These background sources are mostly hadron decaying to muons which survived the tracking requirements for prompt particles.

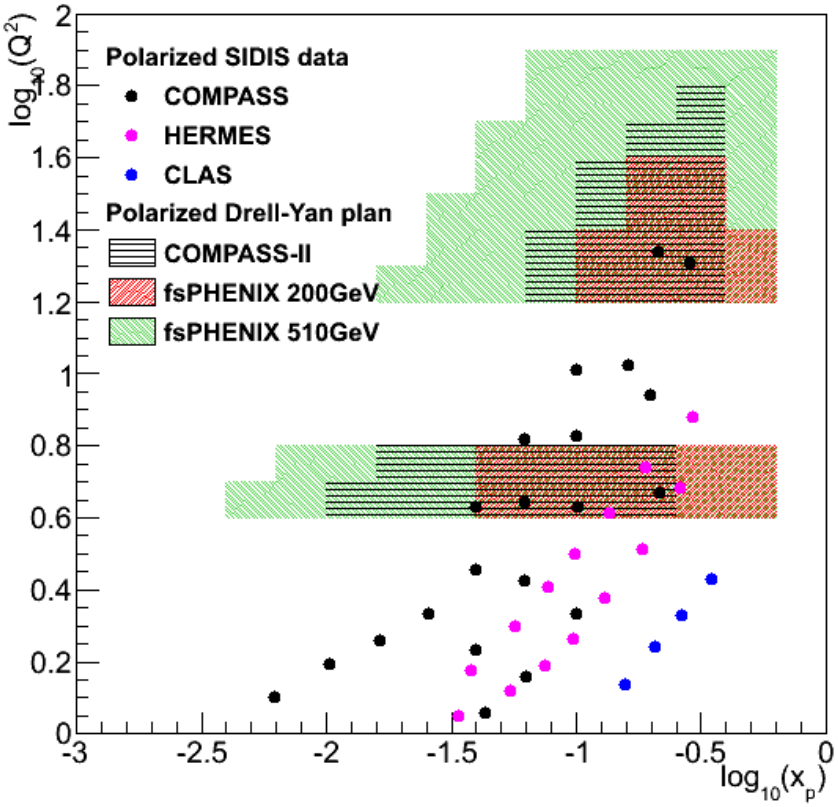

Figure 3.11: The figure shows comparison of Drell-Yan kinematics on x_p vs Q^2 between COMPASS-II and fsPHENIX, and also with existing polarized SIDIS data. The polarized SIDIS data are shown by closed circles and the polarized Drell-Yan plan are shown by closed squares. Each closed square shows a d data point with $\delta A^{\sin\phi_S} < 0.1$.

Both the uncorrelated hadron background and the heavy flavor pairs decrease relative to the Drell-Yan signal as a function of rapidity. Figure 3.16 shows the same invariant mass distributions at 200 GeV with a cut on the pair transverse momentum of $p_T > 2$ GeV. Similar distributions for $p+p$ collisions at 510 GeV are included in Figure 3.17 and Figure 3.18.

In Table 3.5 we list the S/B ratio for the kinematic bins shown in Figures 3.15-3.18.

We emphasize that the mass distributions obtained in Figures 3.15 through 3.18 utilize only the most simple and straightforward analysis cuts and do not yet fully exploit the full power of the fsPHENIX apparatus, particularly for the low mass Drell-Yan region where the higher statistics allow for more restrictive cuts. Taking advantage of the large hadronic calorimeter and tracking coverage of fsPHENIX and sPHENIX (covering $-1 < \eta < +4$), event shape analysis can be used to enhance the Drell-Yan signal to background ratio. Cuts

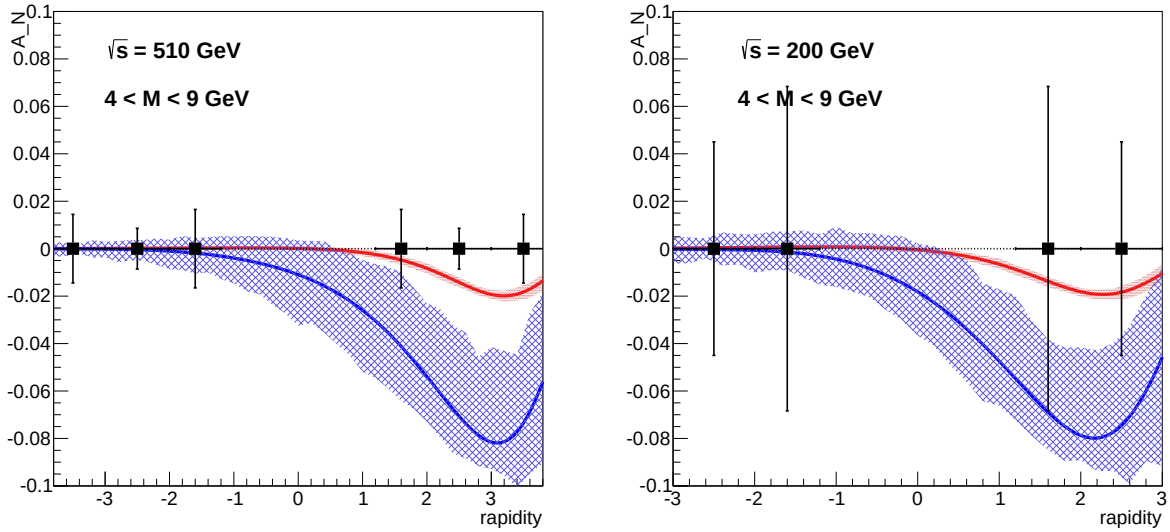

Figure 3.12: Statistical sensitivities of Drell-Yan A_N measurement at fsPHENIX (left panel at $\sqrt{s} = 510$ GeV and right panel at $\sqrt{s} = 200$ GeV) compared with theoretical calculation of the Drell-Yan A_N without Sivers function evolution [50] (blue line and band) and with Sivers function evolution [42] (red line and band).

on five observables have been examined at a preliminary level:

- Summed energy for the hadron calorimeter clusters, whose distance to either of the muon candidate $dR = \sqrt{\Delta\eta^2 + \Delta\phi^2}$ is less than 1.0. The fraction of event which passes a cut for the maximum energy is shown in Figure. 3.19 (a) for the higher invariant mass region in $\sqrt{s} = 510$ GeV proton-proton collisions. At a cut of 9 GeV and a 50% Drell-Yan efficiency, this cut can reject backgrounds by a factor of two to seven.

- The minimal fraction of the transverse momenta of the muon-jet carried by muon, which is similar to the observables used by the LHCb collaboration for a Drell-Yan analysis [51]. Comparing to various background process, Drell-Yan muons are likely to carry higher fraction of transverse momenta. We find its efficiency and rejection is similar to that presented by the hadron calorimeter cut as discussed in the first bullet.

- The minimal azimuthal distance between the opposite side of muon track candidates and the jets, $\Delta\phi_{Back-to-Back} = |\phi_{\text{leading jets}} - (\phi_\mu + \pi)|$. Only The leading and sub-leading jets with $p_T > 2$ GeV/c are considered. The fraction of event passing cut on $\Delta\phi_{Back-to-Back}$ are shown in Figure. 3.19 (b) for the lower invariant mass region in $\sqrt{s} = 510$ GeV proton-proton collisions. With a cut of $\Delta\phi_{Back-to-Back} > 2$, backgrounds can be rejected by two to ten times relative to the signal and 70% of Drell-Yan events will survive the cut.

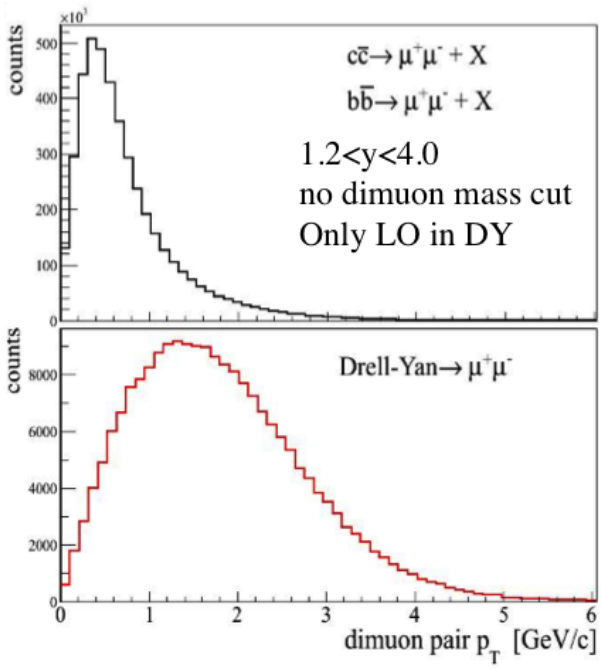

Figure 3.13: The transverse momentum distribution of background pairs from heavy-flavor decay (upper plot) compared with the q_T distribution for Drell-Yan pairs (lower plot). Because Drell-Yan pairs sample higher q_T a cut on the transverse momentum of the pair is an effective way to reduce backgrounds.

- Number of tracks surrounding the muon track candidates. Preliminary studies show this can achieve an additional background rejection of 2–3 at 90% efficiency for Drell-Yan pairs, and four or more at 50% efficiency for Drell-Yan pairs.
- Distance $dR = \sqrt{\Delta\eta^2 + \Delta\phi^2}$ between the muon track candidate and the closest jet. Preliminary studies show this can achieve an additional background rejection of approximately 2 at 90% efficiency for Drell-Yan pairs, and 2–6 at 50% efficiency for Drell-Yan pairs.

These preliminary studies show that by balancing the Drell-Yan pair efficiency against background rejection the S/B ratio for Drell-Yan can be further optimized.

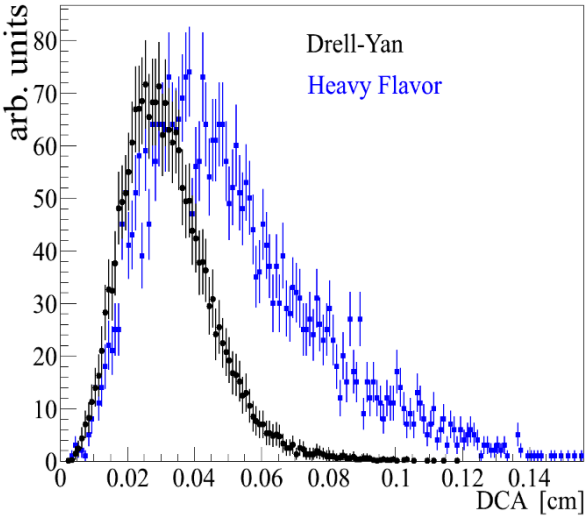

Figure 3.14: Sum of the distance of the closest approach (DCA) of muon pairs from correlated heavy flavor decays and Drell-Yan.

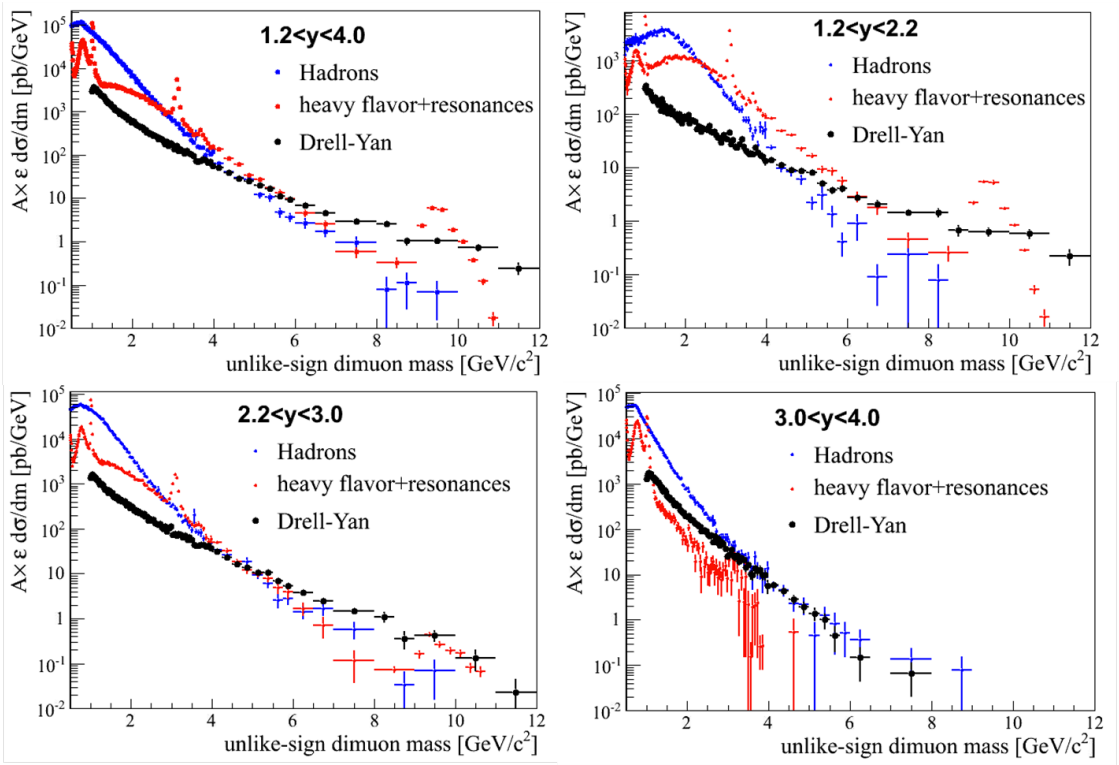

Figure 3.15: Invariant mass of all the unlike-sign pairs from each of generated events from 200 GeV background simulations, as a function of rapidity, and without a cut on the transverse momentum of the pair.

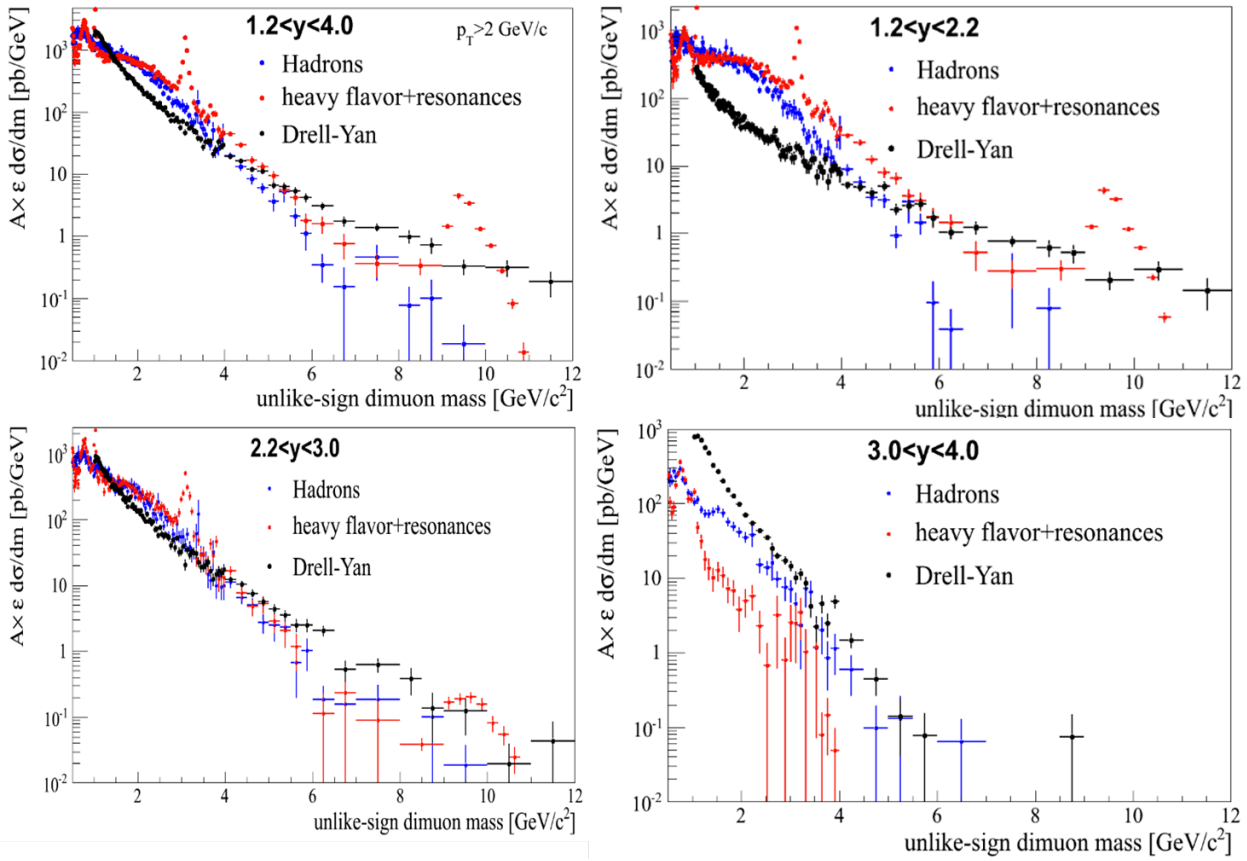

Figure 3.16: Invariant mass of all the unlike-sign pairs from each of generated events from 200 GeV background simulations, as a function of rapidity, and with a $p_T > 2$ GeV/c cut on the transverse momentum of the pair.

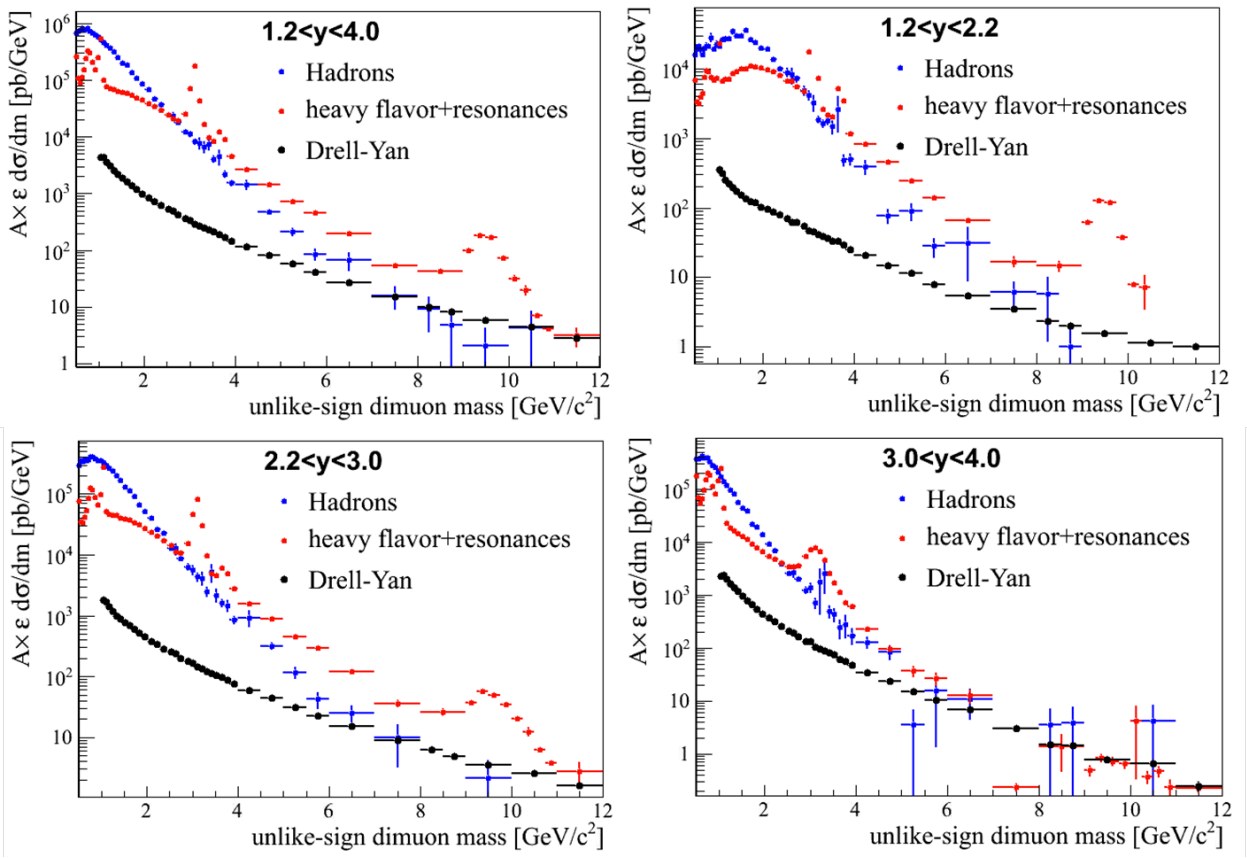

Figure 3.17: Invariant mass of all the unlike-sign pairs from each of generated events from 510 GeV background simulations, as a function of rapidity, and without a cut on the transverse momentum of the pair.

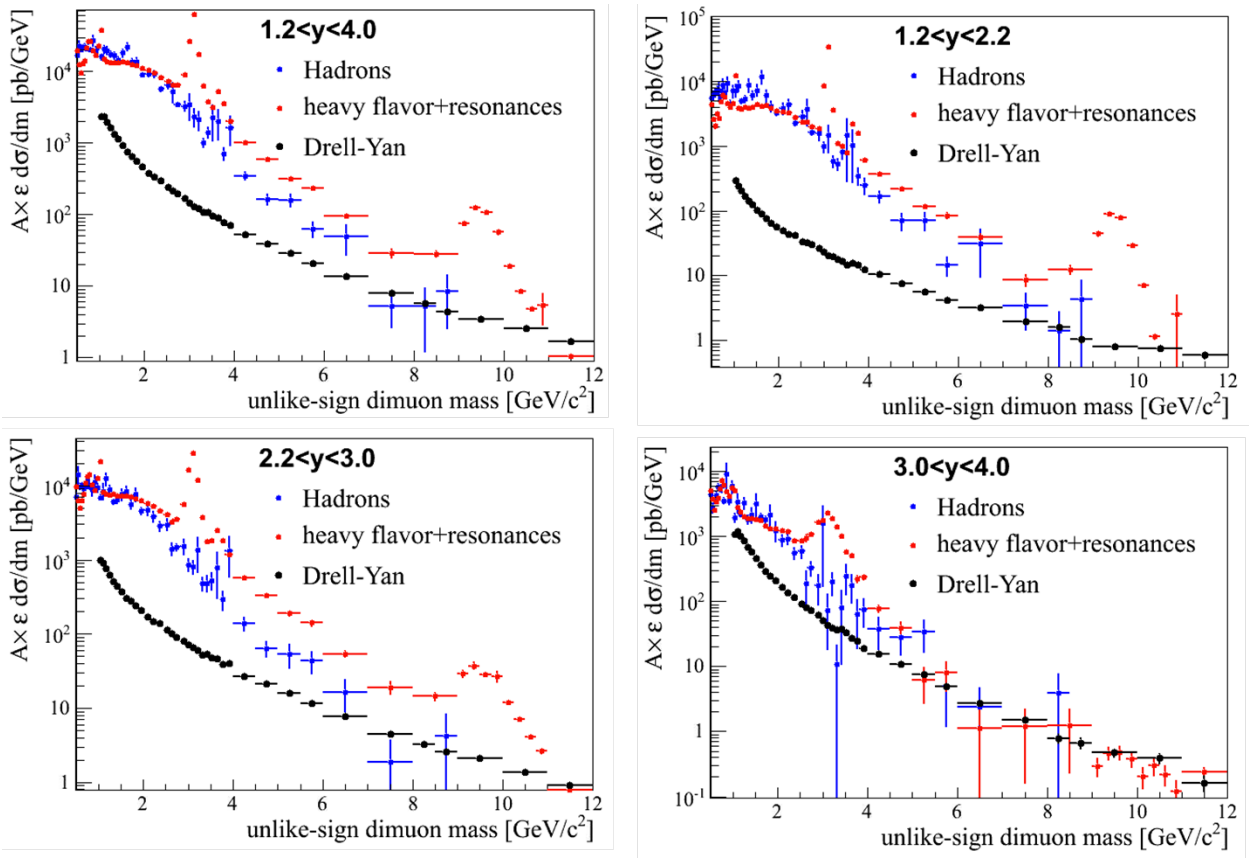

Figure 3.18: Invariant mass of all the unlike-sign pairs from each of generated events from 510 GeV background simulations, as a function of rapidity, and with a $p_T > 2$ GeV/c cut on the transverse momentum of the pair.

Table 3.5: Estimated S/B from background simulations of the fsPHENIX detector in different kinematic regions, corresponding to the results shown in Figures 3.15-3.18. These results use only a basic set of cuts, and do not include event shape cuts.

		$2 < M < 2.5\ GeV/c^2$	$4 < M < 8\ GeV/c^2$
200 GeV	$\mathbf{1.2 < y < 4.0}$:		
	no p_T cut	0.07	0.4
	$p_T > 2\ GeV/c$	0.20	0.5
	$\mathbf{1.2 < y < 2.2}$:		
	no p_T cut	0.04	0.3
	$p_T > 2\ GeV/c$	0.06	0.3
	$\mathbf{2.2 < y < 3.0}$:		
	no p_T cut	0.07	0.6
	$p_T > 2\ GeV/c$	0.25	0.8
	$\mathbf{3.0 < y < 4.0}$:		
	no p_T cut	0.6	0.9
	$p_T > 2\ GeV/c$	1.8	2.3
510 GeV	$\mathbf{1.2 < y < 4.0}$:		
	no p_T cut	0.01	0.05
	$p_T > 2\ GeV/c$	0.02	0.06
	$\mathbf{1.2 < y < 2.2}$:		
	no p_T cut	0.004	0.03
	$p_T > 2\ GeV/c$	0.007	0.03
	$\mathbf{2.2 < y < 3.0}$:		
	no p_T cut	0.007	0.04
	$p_T > 2\ GeV/c$	0.017	0.06
	$\mathbf{3.0 < y < 4.0}$:		
	no p_T cut	0.03	0.15
	$p_T > 2\ GeV/c$	0.07	0.19

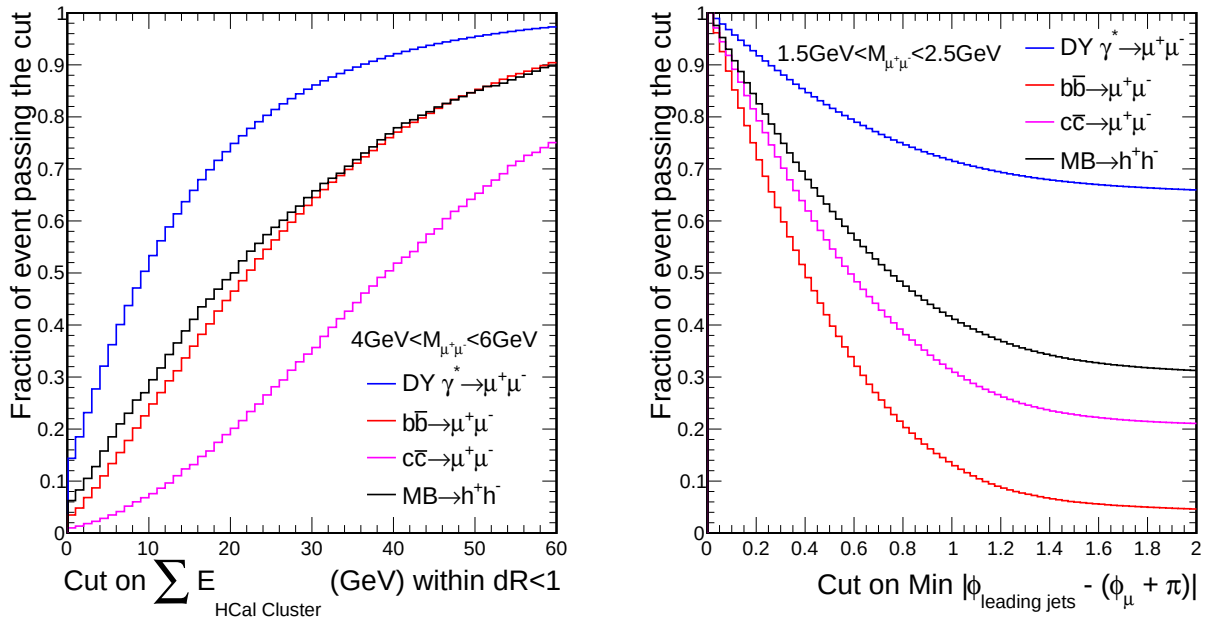

(a) **(b)**

Figure 3.19: For two examples of the event shape cuts, the fraction of event passing the cut plotted against the cut value for Drell-Yan signal (blue), bottom (red), charm (magenta) and hadron backgrounds (black) in $\sqrt{s} = 510$ GeV proton-proton collisions. At a Drell-Yan efficiency of 50%, these cuts can reject different background component by a factor of two to ten relative to the signal.

Chapter 4

Budget

4.1 Cost Estimate

In this chapter we detail a preliminary cost estimate for the fsPHENIX detector. The GEM trackers and hadron calorimeter are included in the EIC detector design [2], hence the cost estimates for these subsystems are taken from the EIC detector design. The cost estimates below include overhead and 50% contingency, and do not include associated estimates for labor costs.

The cost of the other proposed subsystems is based on the cost of similar equipment in PHENIX or other experiments. The cost estimates for fsPHENIX upgrade subsystems are summarized in Table 4.1. The estimates do not include labor costs.

4.1.1 Hadronic Calorimeter

For fsPHENIX we plan to use the same design for the Hadronic Calorimeter as has been developed for the EIC detector in the hadron-going direction, which is a steel-scintillator calorimeter with wavelength shifting fiber and SiPM readout, similar to the sPHENIX central hadronic calorimeter. As from [2], the cost estimate is \$6.87M for HCal detector and \$0.65M for electronics/sensors for $\sim$3000 HCal towers, including overhead and contingency.

4.1.2 GEM Tracker

The GEM tracker planes cost estimate for the EIC detector is done based on the GEM foil cost for CMS detector. The area of the GEM trackers in fsPHENIX is 94% of one proposed for the EIC detector (only hadron-going side trackers will be used in fsPHENIX), hence the EIC detector cost estimate for GEM tracking detector is scaled by this fraction resulting

Table 4.1: Estimated equipment costs for the fsPHENIX upgrade (in $M).

	Cost	Overhead	Contingency	Total
HCal	3.90	0.68	2.29	6.87
GEM Tracker	0.67	0.17	0.41	1.25
FVTX reconfiguration	0.53	0.11	0.31	0.95
miniMUID	0.13	0.03	0.08	0.24
Piston Field Shaper	0.06	0.02	0.04	0.12
HCal electronics/sensors	0.38	0.05	0.22	0.65
GEM electronics/sensors	0.63	0.16	0.39	1.18
miniMUID electronics/sensors	0.05	0.01	0.03	0.09
MUID trigger electronics	0.35	0.07	0.21	0.63
Total	6.7	1.3	3.98	11.98

in a cost of $1.25M, including overhead and contingency. The segmentation of the GEM trackers was assumed to be 1×10 mm^2 pads for inner part and 2×100 mm^2 pads for outer tracker part. This leads to $\sim$200K pads, with $1.18M cost for the whole readout system (based on the CERN SRS readout cost), again including overhead and contingency.

4.1.3 FVTX reconfiguration

The current PHENIX two arms of FVTX detector will be reconfigured into one arm covering $1.2 < \eta < 4$ in fsPHENIX. The silicon detector wedges will be reused and reconfigured into six tracking stations. The estimated cost for the new detector support structures is $430k. With new flexible cables connecting to the detector (cost $370k), the DAQ readout cards inside the IR will be reused, along with the downstream DAQ system. The estimated cost for integrating the new detector with fsPHENIX will be $150k. These estimates are based on the PHENIX FVTX actual cost detailed in FVTX Closeout Report [52] and include overhead, contingency and inflation correction.

4.1.4 Mini-MUID

The current cost estimate is based on the cost of the PHENIX MuID system (in FY97$), corrected for inflation, and scaled to the area of proposed mini-MuID. It resulted in $130k for detectors and $50k for electronics, for which we also included 20% overhead and 50%

contingency in Table 4.1. Additional cost savings may be possible by salvaging part of the south Muon Identifier, which is planned to be removed as part of the sPHENIX installation.

4.1.5 MuID Trigger Electronics

For fsPHENIX we will require new trigger electronics for the MuID detectors capable of real-time tracking on a finer segmentation that the current PHENIX Local Level-1 (LL1) electronics. Because of changes on technology since the MuID detector was first built the existing MuID Readout Controller (ROC) boards that send data over fiber to the LL1 electronics will also require a redesign, as the optical link chipsets required by LL1 to receive the ROC data are no longer available.

We estimate the cost for the LL1 electronics at $200k based on the cost of a similar system design for the PHENIX Muon Trigger upgrade. We estimate an additional $150k for redesign and manufacture of the MuID readout electronics.

4.1.6 Piston Field Shaper

One choice for the large saturation point material for a field shaper could be HIPERCO-50 with a 49%Co+49%Fe. Its market cost is $\sim$\$100/lb. The proposed piston shaper would require $\sim$600 lb of HIPERCO-50, resulting in $60k for the material alone. Extensive simulation studies to quantify the advantages of using tungsten teeth for background suppression, hence at the moment the cost of the tungsten teeth is not included. The cost listed is for materials only and does not include labor or installation costs.

Appendix A

Charge from BNL ALD Berndt Mueller

Charge to RHIC Collaborations: Future opportunities for p+p and p+A at RHIC

The current RHIC run plan anticipates high luminosity Au+Au and p+p runs of RHIC in FY2021 and FY2022 utilizing the enhanced capabilities of sPHENIX and STAR anticipated for these years. The current physics focus of these runs is on hard probes, especially jet observables and Upsilon states. Depending on the available operating funds and presently unknown details of the future run schedule, there may be the opportunity to perform high luminosity p+Au (or other p+A) runs during this time.

C-AD currently anticipates the following peak luminosities: 200 pb^{-1}/week for 500 GeV p+p and 300 nb^{-1}/week for 200 GeV p+Au. The p+p luminosity assumes a bunch intensity of 3×10^{11} up from the present value of 1.85×10^{11}, and shorter bunches. The p+Au luminosity assumes bunch intensities of 3.0×10^{11} for protons and 1.5×10^{9} for Au. Since these numbers represent substantial increases over historically achieved luminosities, it may be prudent to assume somewhat lower numbers for estimates of required beam times.

In view of the prospect that the capability to investigate p+p, p+A, and A+A collisions at RHIC may be lost after the possible transition of the RHIC facility to a electron-ion collider, it is timely to consider the future physics opportunities for a polarized p+p and p+A program at RHIC from our present state of knowledge.

The question of the relative priority of extended p+A runs in the final years of RHIC is likely to come up in the context of the upcoming Long Range Plan process. In order to provide a frame-work for this discussion I am hereby asking the Collaborations to submit Physics Assessments of the scientific reach of such a program in the light of the anticipated capabilities of the RHIC detectors at the time of the final RHIC campaign.

Specifically, I would request that the assessment considers the following issues:

- The scientific motivation for high statistics p+p and p+A data based on our current knowledge, especially in the light of a future EIC physics program and with special consideration of the use of polarized protons;
- What will likely be accomplished during Runs 14-16;
- The compelling physics observables and their expected physics reach;
- The required integrated luminosities;
- The possible need for collision systems other than p+Au (e.g. p+C, p+Cu, d+Au).
- Detector requirements for a successful p+p/p+A program and the associated cost and schedule.

In particular, the document should address which compelling physics questions the p+p and p+A program at RHIC could address in the early part of the next decade in the context of the experiment upgrade plans, the existing and anticipated data from RHIC, LHC, and COMPASS, and a future EIC. The document should address the question to what extent polarized p+p and p+A collisions are complementary to the physics program of an EIC and not just an alternate and possibly less discriminating way of studying the same physics.

In order to be most useful as basis for the discussions in the context of the Long Range Plan process, I request that you submit your assessment no later than April 30, 2014. The two RHIC collaborations may consider the value of collaborating on the physics part of this charge and developing a joint Physics Assessment, followed by separate sections describing the hardware requirements and expected physics reach of each detector.

Berndt Mueller

ALD for Nuclear and Particle Physics

October 8, 2013

Bibliography

[1] C. Aidala et al. sPHENIX: An Upgrade Concept from the PHENIX Collaboration. 2012. arXiv:1207.6378. (document), 2.1, 3.1

[2] A. Adare et al. Concept for an Electron Ion Collider (EIC) detector built around the BaBar solenoid. 2014. arXiv:1402.1209. (document), 2.1, 2.4, 2.6, 3.2.2, 4.1, 4.1.1

[3] Gordon L. Kane, J. Pumplin, and W. Repko. Transverse Quark Polarization in Large p(T) Reactions, e+ e- Jets, and Leptoproduction: A Test of QCD. *Phys.Rev.Lett.*, 41:1689, 1978. doi:10.1103/PhysRevLett.41.1689. 1.1

[4] Jian-wei Qiu and George F. Sterman. Single transverse spin asymmetries in hadronic pion production. *Phys.Rev.*, D59:014004, 1999. arXiv:hep-ph/9806356, doi:10.1103/PhysRevD.59.014004. 1.1

[5] Chris Kouvaris, Jian-Wei Qiu, Werner Vogelsang, and Feng Yuan. Single transverse-spin asymmetry in high transverse momentum pion production in pp collisions. *Phys.Rev.*, D74:114013, 2006. arXiv:hep-ph/0609238, doi:10.1103/PhysRevD.74.114013. 1.1

[6] Yuji Koike and Tetsuya Tomita. Soft-fermion-pole contribution to single-spin asymmetry for pion production in pp collisions. *Phys.Lett.*, B675:181–189, 2009. arXiv:0903.1923, doi:10.1016/j.physletb.2009.04.017. 1.1

[7] Koichi Kanazawa and Yuji Koike. New Analysis of the Single Transverse-Spin Asymmetry for Hadron Production at RHIC. *Phys.Rev.*, D82:034009, 2010. arXiv:1005.1468, doi:10.1103/PhysRevD.82.034009. 1.1

[8] Hiroo Beppu, Koichi Kanazawa, Yuji Koike, and Shinsuke Yoshida. Three-gluon contribution to the single spin asymmetry for light hadron production in pp collision. 2013. arXiv:1312.6862. 1.1

[9] Zhong-Bo Kang, Feng Yuan, and Jian Zhou. Twist-three fragmentation function contribution to the single spin asymmetry in p p collisions. *Phys.Lett.*, B691:243–248, 2010. arXiv:1002.0399, doi:10.1016/j.physletb.2010.07.003. 1.1

[10] A. Metz and D. Pitonyak. Fragmentation contribution to the transverse single-spin asymmetry in proton-proton collisions. *Phys.Lett.*, B723:365–370, 2013. arXiv:1212.5037, doi:10.1016/j.physletb.2013.05.043. 1.1, 1.1

[11] D. Boer et al. Gluons and the quark sea at high energies: Distributions, polarization, tomography. 2011. arXiv:1108.1713. 1.1

[12] Zhong-Bo Kang, Jian-Wei Qiu, Werner Vogelsang, and Feng Yuan. An Observation Concerning the Process Dependence of the Sivers Functions. *Phys.Rev.*, D83:094001, 2011. arXiv:1103.1591, doi:10.1103/PhysRevD.83.094001. 1.1.1

[13] T. Rogers and P. Mulders. No generalized TMD-factorization in the hadro-production of high transverse momentum hadrons. *Phys. Rev.*, D81:094006, 2010. arXiv:1001.2977, doi:10.1103/PhysRevD.81.094006. 1.1.1

[14] Ted C. Rogers. Extra spin asymmetries from the breakdown of transverse-momentum-dependent factorization in hadron-hadron collisions. *Phys.Rev.*, D88(1):014002, 2013. arXiv:1304.4251, doi:10.1103/PhysRevD.88.014002. 1.1.1

[15] L.C. Bland et al. Cross Sections and Transverse Single-Spin Asymmetries in Forward Jet Production from Proton Collisions at $\sqrt{s} = 500$ GeV. 2013. arXiv:1304.1454. 1.1.2

[16] M. Anselmino, M. Boglione, U. D'Alesio, A. Kotzinian, S. Melis, et al. Sivers Effect for Pion and Kaon Production in Semi-Inclusive Deep Inelastic Scattering. *Eur.Phys.J.*, A39:89–100, 2009. arXiv:0805.2677, doi:10.1140/epja/i2008-10697-y. 1.1.2

[17] M. Anselmino, M. Boglione, U. D'Alesio, S. Melis, F. Murgia, et al. Sivers effect and the single spin asymmetry A_N in p(transv. pol.) p $\to$ h X processes. *Phys.Rev.*, D88:054023, 2013. arXiv:1304.7691, doi:10.1103/PhysRevD.88.054023. 1.1.2, 3.2.1

[18] Leonard Gamberg, Zhong-Bo Kang, and Alexei Prokudin. Indication on the process-dependence of the Sivers effect. *Phys.Rev.Lett.*, 110:232301, 2013. arXiv:1302.3218, doi:10.1103/PhysRevLett.110.232301. 1.1.2

[19] K. Abe et al. Measurement of azimuthal asymmetries in inclusive production of hadron pairs in e+ e- annihilation at Belle. *Phys.Rev.Lett.*, 96:232002, 2006. arXiv:hep-ex/0507063, doi:10.1103/PhysRevLett.96.232002. 1.1.3

[20] R. Seidl et al. Measurement of Azimuthal Asymmetries in Inclusive Production of Hadron Pairs in e+e- Annihilation at s**(1/2) = 10.58-GeV. *Phys.Rev.*, D78:032011, 2008. arXiv:0805.2975, doi:10.1103/PhysRevD.78.032011,10.1103/PhysRevD.86.039905. 1.1.3

[21] A. Airapetian et al. Single-spin asymmetries in semi-inclusive deep-inelastic scattering on a transversely polarized hydrogen target. *Phys.Rev.Lett.*, 94:012002, 2005. arXiv:hep-ex/0408013, doi:10.1103/PhysRevLett.94.012002. 1.1.3, 1.3.1

[22] E.S. Ageev et al. A New measurement of the Collins and Sivers asymmetries on a transversely polarised deuteron target. *Nucl.Phys.*, B765:31–70, 2007. arXiv:hep-ex/0610068, doi:10.1016/j.nuclphysb.2006.10.027. 1.1.3, 1.3.1

[23] M.G. Alekseev et al. Measurement of the Collins and Sivers asymmetries on transversely polarised protons. *Phys.Lett.*, B692:240–246, 2010. arXiv:1005.5609, doi:10.1016/j.physletb.2010.08.001. 1.1.3

[24] M. Anselmino, M. Boglione, U. D'Alesio, A. Kotzinian, F. Murgia, et al. Transversity and Collins functions from SIDIS and e+ e- data. *Phys.Rev.*, D75:054032, 2007. arXiv:hep-ph/0701006, doi:10.1103/PhysRevD.75.054032. 1.1.3

[25] M. Anselmino, M. Boglione, U. D'Alesio, S. Melis, F. Murgia, et al. Simultaneous extraction of transversity and Collins functions from new SIDIS and e+e- data. *Phys.Rev.*, D87:094019, 2013. arXiv:1303.3822, doi:10.1103/PhysRevD.87.094019. 1.1.3

[26] Jacques Soffer. Positivity constraints for spin dependent parton distributions. *Phys.Rev.Lett.*, 74:1292–1294, 1995. arXiv:hep-ph/9409254, doi:10.1103/PhysRevLett.74.1292. 1.1.3

[27] I. Arsene et al. Single Transverse Spin Asymmetries of Identified Charged Hadrons in Polarized p+p Collisions at s**(1/2) = 62.4-GeV. *Phys.Rev.Lett.*, 101:042001, 2008. arXiv:0801.1078, doi:10.1103/PhysRevLett.101.042001. 1.1.3

[28] Francois Gelis, Edmond Iancu, Jamal Jalilian-Marian, and Raju Venugopalan. The Color Glass Condensate. *Ann.Rev.Nucl.Part.Sci.*, 60:463–489, 2010. arXiv:1002.0333, doi:10.1146/annurev.nucl.010909.083629. 1.2.1

[29] K.J. Eskola, H. Paukkunen, and C.A. Salgado. EPS09: A New Generation of NLO and LO Nuclear Parton Distribution Functions. *JHEP*, 0904:065, 2009. arXiv:0902.4154, doi:10.1088/1126-6708/2009/04/065. 1.2.1, 1.6

[30] Betty Abelev et al. Transverse Momentum Distribution and Nuclear Modification Factor of Charged Particles in p-Pb Collisions at $\sqrt{s_{NN}} = 5.02$ TeV. *Phys.Rev.Lett.*, 110:082302, 2013. arXiv:1210.4520, doi:10.1103/PhysRevLett.110.082302. 1.2.1

[31] Monika Grothe. Forward physics with CMS. *PoS*, 2008LHC:063, 2008. arXiv:0901.0998. 1.2.1

[32] Z.-B. Kang and F. Yuan. Single Spin Asymmetry Scaling in the Forward Rapidity Region at RHIC. *Phys. Rev.*, **D**84:034019, 2011. arXiv:1106.1375, doi:10.1103/PhysRevD.84.034019. 1.2.2, 1.7

[33] Dennis W. Sivers. Single Spin Production Asymmetries from the Hard Scattering of Point-Like Constituents. *Phys.Rev.*, D41:83, 1990. doi:10.1103/PhysRevD.41.83. 1.3.1

[34] John C. Collins. Fragmentation of transversely polarized quarks probed in transverse momentum distributions. *Nucl.Phys.*, B396:161–182, 1993. arXiv:hep-ph/9208213, doi:10.1016/0550-3213(93)90262-N. 1.3.1

[35] Stanley J. Brodsky, Dae Sung Hwang, and Ivan Schmidt. Final state interactions and single spin asymmetries in semiinclusive deep inelastic scattering. *Phys.Lett.*, B530:99–107, 2002. arXiv:hep-ph/0201296, doi:10.1016/S0370-2693(02)01320-5. 1.3.1

[36] Andrei V. Belitsky, X. Ji, and F. Yuan. Final state interactions and gauge invariant parton distributions. *Nucl.Phys.*, B656:165–198, 2003. arXiv:hep-ph/0208038, doi:10.1016/S0550-3213(03)00121-4. 1.3.1

[37] John C. Collins. Leading twist single transverse-spin asymmetries: Drell-Yan and deep inelastic scattering. *Phys.Lett.*, B536:43–48, 2002. arXiv:hep-ph/0204004, doi:10.1016/S0370-2693(02)01819-1. 1.3.1

[38] M. Anselmino, M. Boglione, U. D'Alesio, S. Melis, F. Murgia, et al. Sivers effect in Drell-Yan processes. *Phys.Rev.*, D79:054010, 2009. arXiv:0901.3078, doi:10.1103/PhysRevD.79.054010. 1.3.1

[39] Zhong-Bo Kang. QCD evolution of naive-time-reversal-odd fragmentation functions. *Phys.Rev.*, D83:036006, 2011. arXiv:1012.3419, doi:10.1103/PhysRevD.83.036006. 1.3.2

[40] S. Mert Aybat and Ted C. Rogers. TMD Parton Distribution and Fragmentation Functions with QCD Evolution. *Phys.Rev.*, D83:114042, 2011. arXiv:1101.5057, doi:10.1103/PhysRevD.83.114042. 1.3.2

[41] Peng Sun and Feng Yuan. Energy Evolution for the Sivers Asymmetries in Hard Processes. *Phys.Rev.*, D88:034016, 2013. arXiv:1304.5037, doi:10.1103/PhysRevD.88.034016. 1.3.2

[42] Miguel G. Echevarria, Ahmad Idilbi, Zhong-Bo Kang, and Ivan Vitev. QCD Evolution of the Sivers Asymmetry. 2014. arXiv:1401.5078. 1.3.2, 3.3, 3.12

[43] C.A. Aidala, B. Field, L.P. Gamberg, and T.C. Rogers. Limits on TMD Evolution From Semi-Inclusive Deep Inelastic Scattering at Moderate Q. 2014. arXiv:1401.2654. 1.3.2

[44] G. Moreno, C.N. Brown, W.E. Cooper, D. Finley, Y.B. Hsiung, et al. Dimuon production in proton - copper collisions at $\sqrt{s}$ = 38.8-GeV. *Phys.Rev.*, D43:2815–2836, 1991. doi:10.1103/PhysRevD.43.2815. 2.2

[45] C. Woody. Future Applications of GEM Detectors at BNL. Technical report, 2013. Talk on RD51 Collaboration Meeting. 2.3.2

[46] P. Abbon et al. The COMPASS experiment at CERN. *Nucl. Instrum. Meth.*, A577:455–518, 2007. arXiv:hep-ex/0703049, doi:10.1016/j.nima.2007.03.026. 2.3.2, 2.7

[47] W. Fisher et al. RHIC Collider Projections (2014-2018). Technical report, BNL, 2013. 3.1, 3.2

[48] A. Adare et al. (PHENIX Collaboration), Measurement of Transverse Single-Spin Asymmetries for forward-rapidity and midrapidity production of mesons in polarized p+p collisions at $\sqrt{s}$ = 200 and 62 GeV, Publication in preparation (2012). 3.2.1

[49] COMPASS-II Proposal, 2010. URL: http://wwwcompass.cern.ch/compass/proposal/compass-II_proposal/compass-II_proposal.pdf. 3.3

[50] Z. Kang and J. Qiu. Single transverse spin asymmetry of dilepton production near Z^0 pole. *Phys. Rev.*, D81:054020, 2010. arXiv:0912.1319, doi:10.1103/PhysRevD.81.054020. 3.3, 3.12

[51] Inclusive low mass Drell-Yan production in the forward region at $\sqrt{s}$ = 7 TeV. 2012. LHCb-CONF-2012-013. 3.3

[52] FVTX Closeout Report. URL: http://www.phenix.bnl.gov/WWW/publish/brooks/silicon/reviews/Apr12CloseOut/Documents/FVTX%20Closeout%20Report.docx. 4.1.3